Supplementary Information to: A comprehensive land surface vegetation model for multi-stream data assimilation

W. Knorr, M. Williams, T. Thum, T. Kaminski, M. Voßbeck, M. Scholze,
T. Quaife, T. L. Smallman, S. Steele-Dunne,
M. Vreugdenhil, T. Green, S. Zaehle,
M. Aurela, A. Bouvet, E. Bueechi, W. Dorigo,
T. El-Madany, M. Migliavacca, M. Honkanen,
Y. H. Kerr, A. Kontu, J. Lemmetyinen, H. Lindqvist, A. Mialon,
T. Miinalainen, G. Pique, A. Ojasalo, S. Quegan, P. Rayner, P. Reyez Muñoz,
N. Rodríguez-Fernández, M. Schwank, J. Verrelst, S. Zhu, D. Schüttemeyer, and M. Drusch

May 23, 2024

Contents

1 Documentation of D&B Model

1.1 Photosynthesis and Autotrophic Respiration

1.1.1 The photosynthesis model

Photosynthesis is computed in two steps. The first is the calculation of the non-water-limited photosynthetic rate, $A_{c,0}$, at a fixed intracellular CO_2 concentration, $C_{i,0}$. Calculation of the actual assimilation rate, A, at the leaf level as a function of the actual intracellular CO_2 concentration, C_i, is here explained for both the C3 and C4 pathway. For C3 plants, following Farquhar et al. (1980), A is formulated as the minimum of an electron transport limited rate, J_E, and a rate, J_C, limited by the carboxylating enzyme Rubisco (in molar units, i.e. mol(CO_2)$m^{-2}s^{-1}$):

$$A = \min\{J_C; J_E\} - R_d \tag{1}$$

with

$$J_C = V_m \frac{C_i - \Gamma_\star}{C_i + K_C(1 + O_x/K_O)} \tag{2}$$

$$J_E = J \frac{C_i - \Gamma_\star}{4(C_i - 2\Gamma_\star)} \tag{3}$$

R_d is the leaf or "dark" respiration (see Section 1.1.2), and J the potential maximum electron transport rate. See Table 2 for oxygen concentration, O_x, and the Michaelis-Mention constants K_C and K_O.

J depends on the rate of PAR absorption, I, in mol photons m^{-2} s^{-1} in the following way:

$$J = \frac{\alpha I J_m}{\sqrt{J_m^2 + \alpha^2 I^2}} \tag{4}$$

where $I = I_{PAR}/E_{PAR}$, with the PAR absorption rate I_{PAR} in W m^{-2} and E_{PAR} the energy content of PAR quanta, (220 kJ/mol, Jones, 1983, p. 160). The temperature dependence of the maximum electron transport rate, J_m, is calculated according to Farquhar (1988) from the canopy temperature, T_v, in ^{o}C and the respective rate at 25^{o}C :

$$J_m(T_v) = J_m(25^o\text{C}) \times T_v/25 \tag{5}$$

The latter is computed from a PFT-specific $V_m(25^o\text{C})$ provided in Table 1 and the average of the ratios provided by Kattge and Knorr (2007) for a range of plants:

$$J_m(25^o\text{C}) = 1.97 \cdot V_m(25^o\text{C}). \tag{6}$$

For the CO_2 compensation point without leaf respiration, $\Gamma_\star$ (in μmol(CO_2)mol(air)$^{-1}$), a linear dependence on vegetation temperature (in ^{o}C) is assumed, again following Farquhar (1988):

$$\Gamma_\star = 1.7 T_v \tag{7}$$

The actual electron transport rate, J_n, required for the SIF observation operator, is limited by J_C, and can computed from

$$J_n = \min\{J_C; J_E\} \frac{4(C_i - 2\Gamma_\star)}{C_i - \Gamma_\star} \quad . \tag{8}$$

At sufficient light, the rate of photosynthesis is limited by V_m, the maximum turnover rate of the primary CO_2 fixating enzyme, Rubisco, while at low light levels, J_m is limiting the assimilation rate. Following Farquhar et al. (1980) and in accordance with Beerling and Quick (1995), a sharp transition from Rubisco to light limited photosynthesis is assumed. In nature, this so-called 'Blackman' curve is observed with a certain transition zone, where both rates

Table 1: D&B vegetation parameters. d_r maximum rooting depth, h_v vegetation height, both in m, V_m maximum carboxylation rate in μmol(CO2)/m^{2}s.

PFT	C3/C4	d_r	h_v	$V_m(25^o\text{C})$
Tropical broadleaf evergreen tree	C3	3.0	30	60
Tropical broadleaf deciduous tree	C3	3.0	15	90
Temperate broadleaf evergreen tree	C3	1.5	15	41
Temperate broadleaf deciduous tree	C3	1.5	15	35
Evergreen coniferous tree	C3	1.0	15	29
Deciduous coniferous tree	C3	1.0	15	53
Evergreen shrub	C3	1.5	1	52
Deciduous shrub	C3	1.5	1	160
C3 grass	C3	0.5	1	42
C4 grass	C4	0.5	1	8
Tundra	C3	0.3	0.3	20
Wetland	C3	0.3	0.3	20
Arable crop	C3	0.3	0.6	117

Table 2: Values of the kinetic parameters and constants for the calculation of the C3 photosynthetic rate with the Farquhar model; lower part: additional constants for C4 photosynthesis. E is the activation energy in J/mol; s.t.: see text, const.: no temperature dependence, F&a: Farquhar et al. (1980), C: Collatz et al. (1992), F: Farquhar (1988), BQ: Beerling and Quick (1995)

symbol	description	value at 25^{o}C	unit	E	reference
α	efficiency of photon capture	0.28	-	(const.)	BQ
$\Gamma_\star$	CO_2 compensation point	42.5	μmol m^{-2} s^{-1}	s.t.	F
O_x	O_2 partial pressure	0.21	mol/mol	35948	F&a
K_C	Michaelis-Menten constant for CO_2	460	μmol/mol	59356	F&a
K_O	Michaelis-Menten constant for O_2	0.33	mol/mol	35948	F&a
V_m	carboxylation capacity	s.t.	μmol m^{-2} s^{-1}	see Table 1	BQ F&a
J_m	electron transport capacity	s.t.	μmol m^{-2} s^{-1}	see Equ. 6	BQ F
R_d	leaf or dark respiration	s.t.	μmol m^{-2} s^{-1}	50967	C
α_i	integrated C4 quantum efficiency	0.04	mol/mol	(const.)	C
k	PEPcase CO_2 specificity	s.t.	mmol m^{-2} s^{-1}	50967	C
θ	curve parameter for J_e	0.83	-	-	C

are simultaneously limiting. The argument used by Farquhar et al. (1980) is that this co-limitation is a suboptimal behaviour that tends to be minimised (Collatz et al., 1990). Nonetheless, a certain co-limitation is often introduced by a curve parameter (e.g Farquhar et al., 1980; Collatz et al., 1991). Because its actual size is difficult to determine for a global simulation, and because the result does not deviate much from that according to Equ. 1, this parameter is not used here.

The values for V_m and J_m are PFT specific for the standard temperature of 25^{o}C (Table 1). α is assigned a value related to incoming light taken from Beerling and Quick (1995) divided by a leaf absorption of 0.86 according to Collatz et al. (1991). The temperature dependence of V_m and all other rates with an activation energy given in Table 2 is computed from the following equation (with T_v in ^{o}C):

$$k(T_v) = k(25^o\text{C}) \exp\left\{\frac{(T_v - 25)E}{298R(T_v + 273)}\right\} \tag{9}$$

where k stands for the rate in question. Rates and constants that do not depend on vegetation type are also listed in Table 2.

In closed canopies, the light-saturated assimilation rate is normally differentiated according to light availability. Therefore, in accordance with Sellers et al. (1996), an exponential reduction in V_m and J_m from top to bottom is assumed for LAI greater than three ($\Lambda > 3$):

$$V_m(l) = V_m \times K_{12} e^{-K_{12} l} \tag{10}$$

$$J_m(l) = J_m \times K_{12} e^{-K_{12} l} \tag{11}$$

where V_m and J_m are the temperature dependent values according to Equs. 9 and 5, and K_{12} the extinction coefficient at noon, according to $K = \frac{1}{2\mu}$ with $\mu = \mu(12{:}00\text{h})$. This scaling of photosynthetic capacity is applied to trees, shrubs and crops, not to grasses or tundra vegetation.

The non-limited or potential photosynthesis rate, A_0, is first calculated from Equ. 1 to 3 with $C_i = C_{i,0}$; then the canopy rate is formed as an integral over the leaf area (cf. Equ. 15):

$$A_{c,0} = \int_0^\Lambda A_0 \left(I_{PAR}(l)\right) dl \tag{12}$$

This integral is solved approximately by summing over several (usually 3) layers, each with PAR absorption, I_{PAR}, calculated separately.

The photosynthetic rate, A, can also be expressed by the following diffusion equation (in mol(CO_2)m^{-2}s^{-1}, e.g. Jones, 1983):

$$A = 0.625 g_s (C_a - C_i) \frac{p}{R T_K}, \tag{13}$$

with air pressure p (from Equ. 124, Section 1.2.8), the ideal gas constant R (8.314 J K^{-1}mol^{-1}), and air temperature in Kelvin T_K ($T_K = T + 273$). The factor 0.625 takes the lower diffusivity of CO_2 against water vapour into account. C_a and C_i are the CO_2 concentrations of free air and of air within the intracellular air spaces in mol(CO_2)/mol(air). The factor behind the brackets is given for the conversion into units of mol(CO_2)/m^3(air) (= 40.9 mol(air)/m^3(air) at 25^{o}C and standard pressure). This equation can now be used to derive the value of stomatal conductance under conditions without moisture stress.

Assuming a typical value for the intracellular CO_2 concentration under such conditions, $C_{i,0}$, the non-water-limited stomatal conductance yields (assuming $g_s = g_{s,0}$):

$$g_{s,0} = \frac{1.6 A_0}{C_a - C_{i,0}} \frac{R T_K}{p}, \tag{14}$$

and after integration across the canopy to obtain canopy conductance:

$$\begin{aligned} G_{c,0} &= \frac{1.6}{C_a - C_{i,0}} \int_0^\Lambda A_0(l) dl \frac{R T_K}{p} \\ &= \frac{1.6 A_{c,0}}{C_a - C_{i,0}} \frac{R T_K}{p} \end{aligned} \tag{15}$$

A dependence of g_s on the following external factors is known (Farquhar and Sharkey, 1982): Light (Sharkey and Ogawa, 1987), intracellular CO_2 concentration (Morison, 1987), potential evapotranspiration, i.e. leaf-to-air gradient of vapour pressure (Fischer and Turner, 1978; Schulze, 1986; Schulze et al., 1987) and soil water content (Schulze, 1986; Turner, 1986; Schulze et al., 1987). According to Schulze et al. (1994), its maximum value, $g_{s,max}$, i.e. the value at sufficient light and water supply, increases with leaf nitrogen content. Since maximum photosynthetic rate, A_{max}, also increases with leaf nitrogen (Field and Mooney, 1986), there is a close relationship between $g_{s,max}$ and A_{max}.

There are two important assumptions contained in this last equation: First, the integrated conductance of a canopy does not, as assumed by Woodward (1987) in a modelling study on water limited LAI, increase linearly with

the leaf area index, Λ. In fact, like $A_{c,0}$, $G_{c,0}$ saturates at high values of LAI, reaching approximately three times the maximum stomatal conductance, $g_{s,0}$. This is the result of a literature review on field measurements by Kelliher et al. (1995). If soil evaporation is also included, the total surface conductance appears to be largely independent of the LAI. The consequence is, that evapotranspiration from vegetated areas is not controlled by LAI, but by the net radiation, R_n. Therefore, a comprehensive description of the energy balance is a prerequisite for mechanistic modelling of the coupled system of evapotranspiration and photosynthesis.

Second, the Equ. 15 suggests a linear relationship between maximum photosynthetic rate and maximum canopy conductance. Such a relationship is the result of an overview by Schulze et al. (1994). Equating the terms "maximum surface conductance" and "maximum canopy CO_2 assimilation" with $G_{c,0}$ and $A_{c,0}$, respectively, the values for C3 plants cited in Schulze et al. (1994) yield

$$G_{c,0} = 0.883 A_{c,0} \tag{16}$$

with $G_{c,0}$ in mm/s and $A_{c,0}$ in μmol(CO_2)m^{-2}s^{-1}. Inserting this into Equ. 15 yields $C_a - C_{i,0} = 45$ ppm or $C_{i,0}/C_a = 0.87$ (at $C_a = 355$ ppm, 25^{o}C and standard pressure), as assumed by the photosynthesis model for conditions without water stress. This is also supported by the common observation that the ratio of leaf internal to external CO_2 concentration stays nearly constant when incident light intensity or external CO_2 concentration changes (Morison, 1987). Therefore, $C_{i,0}$ is set to a uniform value of $C_{i,0} = 0.87 C_a$ for all C3 plants. For C4 plants, this ratio is set to 0.67, based on the relationship for tropical grasses. A lower value for C4 against C3 plants also follows from the different enzyme kinetics of CO_2 uptake, and has been measured regularly, cf. Morison (1987).

Since the leaf or canopy temperature, T_v, depends on the actual rate of transpiration, which in this step has not yet been determined, calculation of $A_{c,0}$ and $G_{c,0}$ up to this point uses the approximation $T_v = T$. A self-consistent calculation, where T_v has to be reinserted iteratively into the equation for $A_{c,0}$, is not carried out here. Since the calculation of $A_{c,0}$ and $G_{c,0}$ at a uniform $C_{i,0}$ has mainly the purpose of formulating a generally applicable dependence of the stomatal conductance on incident light, the error involved is comparatively small, except under significant water stress.

For the second step, the stomatal conductance is modified using the empirical multiplier $1/(1 + b_e \Delta e)$, which is constant across the canopy and therefore applies equally also to $G_{c,0}$ (Equ. 15). Δe is the vapour pressure deficit in the surrounding air (see Section 1.2.9), and b_e an empirical parameter that is set once a day in a way explained in Section 1.2.4. Using this multiplier and the inversion of the diffusion equation for CO_2, we can now determine actual stomatal conductance as

$$\begin{aligned} g_s(l) &= g_{s,0}(l) \frac{1}{1 + b_e \Delta e} \\ &= \frac{1.6 A_0(l)}{C_a - C_{i,0}} \frac{R T_K}{p} \frac{1}{1 + b_e \Delta e} \end{aligned} \tag{17}$$

and actual canopy conductance as:

$$G_c = G_{c,0} \frac{1}{1 + b_e \Delta e}. \tag{18}$$

Once this is known, the water balance of the soil and canopy can be computed as described in Section 1.2.4, and with it the rate of transpiration, E_t (according to Equ. 58) and also the canopy temperature, T_v, as

$$T_v = T + \frac{R_{n,v} - \lambda E_t}{\rho_a c_p G_a}, \tag{19}$$

where $R_{n,v}$ is the net radiation of the canopy (Equ. 126), λ the latent heat of evaporation (Equ. 64), G_a aerodynamic conductance (Equ. 63), and c_p the specific heat of air at constant pressure (≈ 1005 J kg^{-1}K^{-1}). The density of air, ρ_a (≈ 1.29 kg m^{-3}), follows

$$\rho_a = \frac{M_a p}{R T_K} \tag{20}$$

with the molar mass of air ($M_a = 28.964 \times 10^{-3}$ kg mol^{-1}).

The influence of skin reservoir evaporation (E_i) on T_v is neglected here (i.e. $E_v = E_t$).

The actual assimilation rate, A, is eventually computed at a fixed stomatal resistance, g_s, and at a canopy temperature, T_v, computed as described above. The relevant equations are on the one hand Equ. 1 to 3 of the Farquhar model, on the other hand the diffusion equation for CO_2:

$$A(l) = 0.625 g_s(l)(C_a - C_i)\frac{p}{RT_{K,v}}, \tag{21}$$

where $T_{K,v}$ is canopy temperature in Kelvin.

Besides A, the undetermined variable is C_i. Equ. 21 is therefore solved for C_i and inserted into Equ. 2 and 3. The results are quadratic equations for J_C and J_E; the minimum of the respective lesser solutions of those quadratic equations yields $A(l)$. Finally, the canopy photosynthesis, A_c in mol(CO_2)m^{-2}s^{-1}, is taken as the integral over the leaf area:

$$A_c = \int_0^\Lambda A(l)dl = \frac{0.625p}{RT_K}\int_0^\Lambda g_s(l)\left(C_a - C_i(l)\right)dl \tag{22}$$

For C4 photosynthesis, Equ. 1 to 3 are replaced according to Collatz et al. (1992) by the following:

$$A = \min\{J_c; \quad J_e\} - R_d \tag{23}$$

$$J_c = kC_i \tag{24}$$

$$J_e = \frac{1}{2\theta_s}\left[V_m + J_i - \sqrt{(V_m + J_i)^2 - 4\theta_s V_m J_i}\right] \tag{25}$$

$$J_i = \alpha_i \frac{I_{PAR}}{E_{PAR}} \tag{26}$$

As with C3 photosynthesis, a gradual onset of light limitation is assumed, with a sudden transition from J_c to J_e limitation at rising C_i. Another reason for not using a curve parameter for this transition is mathematical: thus, after calculation of $g_s(l)$ as above, $A(l)$ can be derived from:

$$A(l) = \min\left\{J_e; \quad \frac{C_a + R_d/g_s'(l)}{1/k + 1/g_s'(l)}\right\} - R_d \tag{27}$$

with $g_s' = 0.625 g_s p/(RT_{K,v})$.

1.1.2 Autotrophic respiration

Following Farquhar et al. (1980), leaf or dark respiration, R_d, per leaf area at 25^{o}C is assumed proportional to V_m, also at 25^{o}C. The constant of proportionality depends on photosynthetic pathway and is 0.011 for C3 plants (Farquhar et al., 1980; Collatz et al., 1991). For C4 plants we expect a higher value owing to the more complex two-step photosynthetic system. Therefore, the value for C4 grasses is chosen such as that simulated GPP and NPP for C3 and C4 grasses are equal in areas where they were found to be equally abundant. C3 and C4 grass GPP, NPP and abundance were calculated by Knorr (1997), with abundances based on Paruelo and Lauenroth (1996).

The resulting formulation for leaf respiration used here is:

$$R_d(25^o\text{C}) = \begin{cases} 0.011 V_m(25^o\text{C}) & \text{(C3)} \\ 0.042 V_m(25^o\text{C}) & \text{(C4)} \end{cases} \tag{28}$$

The temperature dependence of R_d is again given by Equ. 9 with an activation energy according to Table 2.

Following Ryan (1991a), total plant or autotrophic respiration, R_A, is divided into two parts, maintenance (R_M) and growth respiration (R_G):

$$R_A = R_M + R_G. \tag{29}$$

The difference between the two is that the so-called growth respiration occurs only when NPP > 0. $R_{d,c}$ is the integral of R_d over the differential leaf area index, l:

$$R_{d,c} = \int_0^\Lambda R_d(l)dl \tag{30}$$

and is assumed to constitute a large part of R_M. Λ is the total leaf area index (LAI). As explained in Section 1.1.3, the integral is approximated by a fixed number of discrete layers.

Ryan (1991a) stresses that R_M and the nitrogen content of vegetation, N_{tot}, are usually much better correlated than R_M and biomass, with R_M approximately 0.30μmol(CO_2)$m^{-2}s^{-1}$ per gN at 25^{o}C , if we assume the same temperature dependence as for R_d. Since V_m is nearly proportional to the nitrogen content of leaves (Farquhar et al., 1980) with around 45μmol(CO_2)$m^{-2}s^{-1}$ per gN (at 25 ^{o}C, with 20% of N in Rubisco), it follows from Equ. 28 for C3 plants that R_d is approximately 0.5μmol(CO_2)$m^{-2}s^{-1}$ per gN, somewhat more than R_M. It seems that leaves, in terms of their nitrogen content, take up a higher proportion of total plant respiration than the remaining plant parts. Further, from the data by Ryan (1991b) it follows that typically 40% of maintenance respiration takes place in the leaves. For this reason, the following equation is used:

$$R_M = M_c R_{d,c}/f_{R,leaf} = 1.67 M_c R_{d,c}/f_{N,leaf} \tag{31}$$

$f_{R,leaf}$ is the leaf fraction of the plant-total maintenance respiration, and $f_{N,leaf}$ the leaf fraction of total nitrogen. The factor 1.67 accounts for the higher respiration rates per N in leaves, while the factor $M_c = 12$ gC/mol(CO_2) is used because photosynthesis is expressed in molar units of carbon.

In a subtropical dry forest in Puerto Rico (Lugo and Murphy, 1986), leaf nitrogen was 189 kg/ha of a total of 916 kg/ha, i.e. 21%, whereas in an equatorial moist forest in Zaïre (a 28-year-old secondary forest) 143 kg/ha were found in leaves for a 593 kg/ha total (Greenland and Kowal, 1960), this is a portion of 24%. (With Equ. 31, this would mean $f_{R,leaf} \approx 0.4$). The similarity contrasts with the fact that with 25%, the root fraction of total nitrogen was significantly lower in the moist than in the dry forest, where it amounted to as much as 60%. It appears that the value of $f_{N,leaf}$ is a conservative quantity compared to the distribution of biomass between leaves, stem and roots. A possible explanation is that trees, because of competition with other trees, accumulate woody biomass until a certain critical value of $f_{N,leaf}$ around 20 to 25% is reached, from where on a reduction in NPP prevents further reduction of the relative leaf fraction. This might also be true for grasses, which increase root biomass under arid conditions until a similar value of $f_{N,leaf}$ is reached. This would explain why respiration costs relative to GPP are remarkably similar for grasses and trees (Ryan, 1991a). Therefore, in this study a uniform value of $f_{N,leaf} = 0.14$ will be used, or $f_{R,leaf} = 0.40$.

A mean value for growth respiration according to Ryan (1991a), which will be used here, is 0.25 gC per gC biomass produced, or $f_{R,G} = 0.25$. Using

$$\mathrm{NPP} = \mathrm{GPP} - R_M - R_G \tag{32}$$

We can thus derive an implicit equation for

$$R_G = f_{R,G} \cdot \mathrm{NPP} = f_{R,G}(\mathrm{GPP} - R_M - R_G), \tag{33}$$

which yields the following explicit form:

$$R_G = \frac{f_{R,G}}{1 + f_{R,G}}(\mathrm{GPP} - R_M) \tag{34}$$

The equation for net primary productivity thus becomes:

$$\mathrm{NPP} = \frac{1}{1 + f_{R,G}}(\mathrm{GPP} - R_M). \tag{35}$$

1.1.3 Light absorption

Light absorption in the photosynthetically active spectrum is calculated within the two-flux approximation, following Sellers (1985), expressed by the following equations (with the cumulative leaf area index, l, as the vertical coordinate, where $l = 0$ at the top, and $l = \Lambda$ at the bottom of the canopy):

$$\begin{aligned} \bar{\mu}\frac{dR_\downarrow}{dl} + [1-(1-\beta)\omega]R_\downarrow - \omega\beta R_\uparrow &= \omega\bar{\mu}K(1-\beta_0)R(l) \\ -\bar{\mu}\frac{dR_\uparrow}{dl} + [1-(1-\beta)\omega]R_\uparrow - \omega\beta R_\downarrow &= \omega\bar{\mu}K\beta_0 R(l) \end{aligned} \tag{36}$$

$R_\downarrow$ and $R_\uparrow$ are the diffuse fluxes downward and upward, respectively, and $R(l)$ is the direct flux with $R(0) = d_{PAR}R_{PAR}$ (Equ. 111 and 122):

$$R(l) = R(0)e^{-Kl} \tag{37}$$

Further, ω is the leaf single scattering albedo, β the forward scatter fraction for the diffuse flux, β_0 the same for the direct flux, K the extinction coefficient for the direct flux and $\bar{\mu}$ the mean of K^{-1} over the downward hemisphere ($\int_0^1 K^{-1}(\mu)d\mu$).

The following simplifications are used: (1) There is no preferred leaf orientation, i.e. distribution of leaf angles is isotropic; (2) leaf reflectivity and transmissivity are equal (the sum of the two is ω). These assumptions yield:

$$\beta = \frac{1}{2} \tag{38}$$

$$\beta_0 = \frac{1}{2} \tag{39}$$

$$K = \frac{1}{2\mu} \tag{40}$$

$$\bar{\mu} = 1 \tag{41}$$

where μ is the cosine of the solar zenith angle (cf. Equ. 109).

The following boundary conditions are also needed for the solution of Equ. 36: (1) $R_\downarrow(0)$ equals diffuse incoming radiation; (2) the reflection at the lower boundary is given by the soil reflectivity in the PAR region, ρ_s^{PAR}:

$$R_\downarrow(0) = (1-d_{PAR})R_{PAR} \tag{42}$$

$$R_\uparrow(\Lambda) = \rho_s^{PAR}\left(R(\Lambda) + R_\downarrow(\Lambda)\right) \tag{43}$$

The standard value for the single scattering albedo for PAR is set to $\omega = 0.12$, while ρ_s^{PAR} is computed from the soil albedo in the total solar spectrum, ρ_s:

$$\rho_s^{PAR} = 0.92\rho_s - 0.015 \tag{44}$$

This dependence has been derived from the "soil line" by Price and Bausch (1995), a linear relationship between PAR and NIR (near infrared) reflectivity for moist soils, with the assumption $\rho_s = (\rho_s^{PAR} + \rho_s^{NIR})/2$ (cf. Section 4.5).

The rate of PAR absorption per leaf area of layer k, I_k^{PAR}, is calculated, to be used for the light limited photosynthetic rate (Equ. 3), as the sum over N_l layers of equal distance in l-coordinates, going from $l = l_{k-1}$ to $l = l_k$ with $l_0 = 0$ and $l_{N_l} = \Lambda$:

$$\begin{aligned} I_k^{PAR} &= \frac{1}{l_k - l_{k-1}}\int_{l_{k-1}}^{l_k}\left\{-\frac{d}{dl}(R + R_\downarrow + R_\uparrow)\right\}dl \\ &= \{[R(l_{k-1}) + R_\downarrow(l_{k-1}) - R_\uparrow(l_{k-1})]\ldots \\ &\quad \ldots - [R(l_k) + R_\downarrow(l_k) - R_\uparrow(l_k)]\}/(l_k - l_{k-1}) \end{aligned} \tag{45}$$

where R, $R_\downarrow$ and $R_\uparrow$ are the solutions to the Equ. 36, 42 and 43 with LAI Λ. The canopy photosynthesis is then

$$A_c = f_c \sum_{k=0}^{N_l} A(I_k^{PAR}) \quad (l_k - l_{k-1}) \tag{46}$$

and FAPAR can be calculated from

$$\begin{aligned} f_{PAR} &= \{[R(0) + R_\downarrow(0) - R_\uparrow(0)] - [R(\Lambda) + R_\downarrow(\Lambda) - R_\uparrow(\Lambda)]\} / (R(0) + R_\downarrow(0)) \\ &= 1 - \frac{R_\uparrow(0) + (1 - \rho_s^{PAR})(R(\Lambda) + R_\downarrow(\Lambda))}{R(0) + R_\downarrow(0)} \end{aligned} \tag{47}$$

Equ. 46 is the approximation used for the integrals of Equ. 12 and 22. Following the arguments by Sellers (1985), no separate layer for sunlit leaves is introduced.

1.2 Energy and Water Cycle

1.2.1 Water balance overview

The model considers a total of three water pools: soil water (W_s), a skin or intercepted reservoir on leaves and other plant parts (W_i) and snow (W_{sn}). The total amount of water at the surface, W_{tot}, from Equ. 51, is thus partitioned into three components (cf. Equ. 52, 53 and 98):

$$W_{tot} = W_s + W_i + W_{sn} \tag{48}$$

The largest part by far is W_r, the root-zone soil moisture. There is also an additional thin soil layer at the surface, W_s, which, however, overlaps with the root-zone soil moisture layer. The other two components are the intercept pool (W_i), and the snow pool (W_{sn}). The precipitation rate, P_{tot}, and the rate of evapotranspiration, E_{tot}, are also divided into further quantities:

$$P_{tot} = P_s + P_i + P_{sn} \tag{49}$$

and

$$E_{tot} = E_s + E_{sn} + E_i + E_t \tag{50}$$

Here, P_s is the amount of rain falling directly on the soil, P_i the part intercepted by vegetation and P_{sn} the rate of snowfall. The partitioning of total precipitation, P_{tot}, into snow (P_{sn}) and rain ($P_r = P_s + P_i$) is calculated from Equ. 99 (see Section 1.2.7) and the interception rate, P_i, according to Equ. 54 (see Section 1.2.3). There is also an indirect "rain" rate, P_v, of water that overflows from the leaf surfaces and drips down to the floor (Equ. 55). The components of total evapotranspiration are E_s (soil evaporation, Equ. 83), E_{sn} (snow evaporation, Equ. 103), E_i (evaporation from the intercepted skin reservoir, Equ. 60), and E_t (transpiration, Equ. 62).

The water balance can be described by the following equation:

$$P_{tot} - E_{tot} - Q_d - Q_b = \dot{W}_{tot} \tag{51}$$

P_{tot} is the total precipitation rate, E_{tot} the total evapotranspiration from soil, leaf surfaces, through leaf pores and from snow (including sublimation), W_{tot} the total amount of water stored in the soil, on the vegetation and on the ground as snow, Q_d is direct runoff, and Q_b base flow.

1.2.2 Root-zone soil water balance

The root-zone soil water balance can be expressed as

$$W_r(t) - W_r(t - \Delta t) = (P_s(t) + P_v(t) + S_m(t) - E_t(t) - E_s(t) - Q_b(t))\Delta t \tag{52}$$

with a time step Δt of one day. The flux terms on the right hand side of the equation are therefore daily averages in kg m^{-2}s^{-1}. P_s and P_v are, respectively, the precipitation rates arriving at the soil directly, or being intercepted by vegetation first and then dripping through to the ground. P_s is calculated from $P_s = P - P_{sn} - P_i$ with P_{sn} from Equ. 99 and P_i from Equ. 54; P_v is given by Equ. 55 (Section 1.2.3), S_m, the rate of snow melt, by Equ. 100 (Section 1.2.7), E_t by Equ. 62 (transpiration, Section 1.2.4) and E_s by Equ. 83 (soil evaporation, Section 1.2.5). $Q_b(t)$ is the base flow, which is proportional to the root-zone soil moisture and capped to zero when the root-zone soil moisture is less than the field capacity.

1.2.3 Skin water balance

The balance equation of the skin or intercepted reservoir, W_i, is

$$W_i(t) - W_i(t - \Delta t) = (P_i(t) - E_i(t) - P_v(t))\Delta t \tag{53}$$

If rain falls on dense vegetation (approx. LAI > 3), most of it falls on leaves and branches. A considerable fraction initially remains as a thin film on the vegetation, while another fraction, depending on the size of raindrops and the interception capacity of the canopy, reaches the ground. While rainfall continues, the skin reservoir, W_i, reaches a maximum and the water begins to drip through to the ground. A good approximation for the LAI dependence of interception is the vertical projection of the leaf area divided by the ground area. When this value approaches 1, it is assumed that 100% of rainfall is intercepted by the vegetation canopy:

$$P_i = f_c \left(1 - e^{-0.5\Lambda/f_c}\right) P_r \tag{54}$$

f_c is the fractional cover of vegetation and Λ the LAI of the total area (vegetated and non-vegetated). Finally, the daily throughfall of rain through the canopy, $P_v\Delta t$, is calculated according to:

$$P_v\Delta t = \max\left\{W_i(t - \Delta t) + P_i\Delta t - W_{i,max};\quad 0\right\} \tag{55}$$

Thereby it is assumed that the skin reservoir fills up to a capacity of $W_{i,max}$ and that no evaporation happens during rain. The interception capacity of the vegetation, $W_{i,max}$, is assumed proportional to LAI as in the BATS model (Dickinson et al., 1993)

$$W_{i,max} = w_{i,max}\Lambda \tag{56}$$

with an area-specific capacity, $w_{i,max}$, of 0.1 kg m^{-2}. Because of $W_i(t) \geq 0$, the daily evaporation from the skin reservoir is limited by the sum of the rain input and the size of the reservoir:

$$E_i\Delta t \leq (P_i - P_v)\Delta t + W(t - \Delta t)$$

This is taken into account in Equ. 60 when computing E_i.

1.2.4 Evaporation from vegetation

Total evapotranspiration from vegetation ($E_v = E_t + E_i$) is primarily driven by the net radiative balance of the vegetation ($R_{n,v}$, Equ. 126) and is limited by the available amount of soil (W_s, Equ. 52) and skin water (W_i, Equ. 53). If the vegetation surfaces are wet ($W_i > 0$), the canopy conductance is infinite ($G_c \to \infty$) so that evaporation follows its maximum rate, $E_{v,max}$, with the evaporated water coming from the skin reservoir:

$$E_v = E_i = E_{v,max} = \frac{sR_{n,v} + \rho_a c_p(e_s(T) - e_a)G_a}{s + \gamma} \qquad (W_i > 0) \tag{57}$$

Here, E_i is allowed to assume negative values during dew formation. When the vegetation is dry ($W_i = 0$), evapotranspiration is determined by G_c, which is the combined conductance of all stomata within the plant canopy. The transpiration rate is then calculated from the Penman-Monteith formula (Monteith, 1965):

$$E_v = E_t = \frac{sR_{n,v} + \rho_a c_p (e_s(T) - e_a) G_a}{s + \gamma(1 + G_a/G_c)} \qquad (W_i = 0) \tag{58}$$

An additional condition is given by $E_t \geq 0$, i.e. transpiration is only allowed from the vegetation to the atmosphere.

Here, γ is the psychrometric constant (≈ 65 Pa K^{-1}), defined as

$$\gamma = \frac{pc_p}{0.622\lambda}. \tag{59}$$

e_a is vapour pressure of air (see Equ. 141), e_s saturated vapour pressure, and s the strongly temperature dependent slope of the vapour pressure curve, $\partial e_s(T)/\partial T$ (see Equ. 144, for rho_a see Equ. 20).

The daily integral of the evaporation rate E_i also depends on the size of the skin reservoir, W_i, and the rain input:

$$E_i(t)\Delta t = \min \left\{ \int_{1 \text{ day}} E_{v,max}(t')dt'; \quad W_i(t - \Delta t) + (P_i(t) - P_v(t))\Delta t \right\} \tag{60}$$

with a one-day time step Δt. In the model, this and all other daily integrals are approximated by summing up hourly values of the instantaneous rates.

According to Equ. 58, transpiration can only happen when the vegetation is dry. To account for this fact when calculating the daily rate $E_v \Delta t$, a time average wetness fraction is defined:

$$\mathcal{F}_i = \frac{E_i(t)\Delta t}{\int_{1 \text{ day}} E_{v,max}(t')dt'} \tag{61}$$

and daily transpiration is reduced accordingly:

$$E_t(t)\Delta t = (1 - \mathcal{F}_i) \int_{1 \text{ day}} \frac{sR_{n,v} + \rho_a c_p \Delta e G_a}{s + \gamma(1 + G_a/G_c)} dt \tag{62}$$

The canopy conductance, G_c, is computed from Equs. 15 and 18 as described in Section 1.1.1. The aerodynamic conductance, G_a, between the canopy and a reference height of 10 m is estimated from vegetation height, h_v (from Table 1):

$$G_a = \frac{\kappa u}{\left[\ln(\frac{10}{0.1h_v} + 1)\right]^2} \tag{63}$$

with h_v in metres, a roughness length of $0.1h_v$ and a wind speed, u, 10 m above the canopy. u is set to a uniform value of 2 m/s, and κ is the von Karmann constant (0.41). For temperate broadleaf and coniferous forests ($h_v = 15$ m), this amounts to a value for G_a of 0.198 m/s, while for short grass ($h_v = 0.3$ m, Table 1) it is 0.024 m/s, in good agreement with the average observed values in Kelliher et al. (1993).

Further, , and λ the latent heat of evaporation (2.45 MJ kg^{-1}at 20^{o}C). Since snow sublimation is also modelled, e_s, s and λ are calculated differently for temperatures above or below 0^{o}C, e_s and s according to Equ. 144, and λ (in J kg^{-1}, with T in ^{o}C) from

$$\lambda = \begin{cases} 2.501 \times 10^6 - 2.38 \times 10^3 T & \text{for} \quad T > 0^o\text{C} \\ 2.834 \times 10^6 & \text{for} \quad T < 0^o\text{C} \end{cases} \tag{64}$$

Table 3: Results of a curve fit of $g_s = g_0/(1 + b_e\Delta e)$ to measurements by Turner et al. (1984), after minimising the root mean squared (r.m.s.) difference between curve and measurements. g_0 is in mmol m^{-2} s^{-1}, b_e in kPa^{-1}.

Species	g_0	b_e	r.m.s.	n
Helianthus annus	707	0.35	9.5	5
Vigna unguiculata	2161	3.23	13.7	4
Pistacia vera	606	0.85	11.7	5
Nerium oleander	344	0.39	12.1	5
Prunus dulcis	209	0.39	6.4	5

with a slightly temperature dependent evaporation heat (Jones, 1983) and a fixed sublimation heat (Anderson, 1976).

With Equ. 15, the potential transpiration rate is now defined:

$$\lambda E_{t,max} = \frac{sR_{n,v} + \rho_a c_p \Delta e G_a}{s + \gamma(1 + G_a/G_{c,0})} \tag{65}$$

This value is called "demand" by Federer (1979) and is equal to the transpiration rate without water limitation (see above, Equ. 65).

Calculation of the actual canopy conductance, G_c, and the actual transpiration rate, E_t, follows a combination of the approaches by Jarvis (1976) and Federer (1982). There is only one empirical multiplicative factor depending on vapour pressure deficit, $\Delta e = e_s(T) - e_a$, and with a functional form proposed by Lindroth and Halldin (1986) (see also Section 1.1.1):

$$G_c = G_{c,0}\frac{1}{1 + b_e\Delta e} \tag{66}$$

A test of this form with measurements by Turner et al. (1984) is shown in Table 3. A curve described by $g_s = g_0/(1 + b_e\Delta e)$ with two free parameters is fitted by minimising the root mean squared (r.m.s.) deviation from the measurement. The success of the test is documented by the fact that the deviation is always much smaller than g_0.

Studies by Turner et al. (1984) and Schulze et al. (1987) suggest that a signal transmitted by hormones from the roots is responsible for the closing of stomata under water limitation. To account for this effect, another multiplicative factor could be added to Equ. 66, as in the Jarvis approach. This would mean that stomata close even under sufficient water supply as a reaction to rising vapour pressure deficit. However, stomata do not react directly to vapour pressure deficit of the surrounding air, but to a rise in the evaporative demand (Schulze et al., 1987); as long as the supply of soil water is sufficient, stomata tend to remain open even under high atmospheric drought.

A different approach is therefore chosen here, following Federer's model: The empirical constant b_e is redefined at each daily integration such that at the time of the highest transpirational demand, $E_{t,max}$, assumed at 13:00 hours in the model, the transpiration rate from Equ. 58 is less or equal to a supply rate, S. This rate is constant over a day and depends on soil water content and root density. Without detailed knowledge of soil hydrology and root distribution, a reasonable approximation according to Federer (1982) is

$$S = c_w\frac{W_s^{eff}}{W_{s,max}} \tag{67}$$

with values for c_w in the range of 0.5 to 2.0 mm/hour and an effective soil water content, W_s^{eff} (Equ. 68). In particular, $b_e = 0$ if demand, $E_{t,max}$, is less than S throughout the day.

Thus, the only remaining free parameter of the stomatal model is the rate c_w. This is justified by the fact that this parameter represents the root system that is not described explicitly. All other elements of the model are based on general principles of stomatal control or on empirical findings. An empirical approach is chosen in Equ. 66 instead of

a mechanistic description of stomatal response to atmospheric demand (Schulze et al., 1987; Friend, 1995), because designing a global model of detailed soil hydraulic processes appears to be unfeasible. Sensitivity tests by Knorr (1997) have shown that global carbon and water fluxes are rather insensitive to the choice of c_w, which are mostly contrained by the available soil water and atmospheric CO_2 content.

The last point described in this subsection is the dependence of stomatal conductance on soil and air temperature as assumed in the model: On the one hand, the temperature dependence of G_c is given by the temperature dependence of $A_{c,0}$ through Equ. 15. Also, $A_{c,0} = 0$ if the daily average of air temperature, $\bar{T}$, is zero degrees or less, and thus $G_c = 0$ and $E_t = 0$. On the other hand, if the soil is partly frozen while the air is already warmer than 0^{o}C, there is a dependence on soil temperature through the effective plant available soil water fraction, f_{soil}^{eff} (cf. f_{soil} Equ. 92)

$$f_{soil}^{eff} = \begin{cases} \max\left\{f_{soil}\left(1 - \frac{d_{fr}}{d_r}\right); 0\right\} & \text{if} \quad \bar{T} > 0 \quad \text{and} \quad \bar{T} > \bar{T}_{ds} \\ 0 & \text{if} \quad \bar{T} < 0 \\ f_{soil} & \text{else.} \end{cases} \tag{68}$$

d_r is the rooting depth (Table 1), $\bar{T}_{ds}$ the daily mean soil temperature (subscript "ds" for deep soil) at depth d_{ds}, and d_{fr} the frost penetration depth.

To determine the frost depth, d_{fr}, a linear temperature course is assumed up to the surface. With this assumption, d_{fr} can be computed for the first case in Equ. 68:

$$d_{fr} = \frac{d_{ds}\bar{T}}{\bar{T} - \bar{T}_{ds}} \tag{69}$$

$\bar{T}_{ds}$ is one of the driving variables, see Section 1.4. The depth for which soil temperatures are available varies by driving data set, but should be similar to rooting depth. In the current model implementation we assume d_{ds}=1.50 m.

The following effect is neglected in the model described here: When calculating net radiation of vegetation, $R_{n,v}$, or soil, $R_{n,s}$, longwave upward radiation after Equ. 129 is calculated from air instead of skin temperature. For example, the skin temperature of vegetation, T_v, depends itself on the sensible heat flux $H_v = R_{n,v} - \lambda E_v$. To a linear approximation, this can be accounted for by the concept of isothermal conductivity, G_i (e.g. Jones, 1983), that has to be added to the surface conductivity. Its value can be calculated from $G_i = 4\sigma T^4 t_{l,v}/(pc_p M_a)$, which is 3.5 mm/s at 0^{o}C and 6.0 mm/s at 40^{o}C, $p = p_0$ and $t_{l,v} = 1$. This is an order of magnitude smaller than G_a for a typical grassland and even two orders of magnitude for coniferous forests (Kelliher et al., 1993), so that G_i can generally be neglect in large-scale studies.

To close the energy balance given by Equ. 96 and 97, the calculation of the sensible heat flux, H, is also explained:

$$\begin{aligned} H &= H_v + H_s \\ &= R_n - G - \lambda E_{tot} \\ &= R_{n,v} + R_{n,s} - G - \lambda(E_t + E_i + E_s + E_{sn}) \end{aligned} \tag{70}$$

1.2.5 Soil water module

The following description of the soil water balance is taken to a large extent from Scholze et al. (2016). Soil evaporative demand is assumed according to equilibrium evapotranspiration calculated using the net radiation of the soil (Equ. 97). Actual soil evaporation and the balance of soil water inputs and outputs follow the 1-layer version of the Variable Infiltration Capacity (VIC-1L) model (Wood et al., 1992).

The assumptions made by VIC-1L are as follows:

- The total soil water column that can be stored at a given place within a grid cell until the soil is saturated, denoted i, has some statistical distribution $f(i)$ between the values 0 and i_m.

- The present soil water content at some location within the grid cell is either at saturation, or assumes a value i_0 that is uniform for all locations accept those that are saturated, i.e. where i_m is reached.
- Rain falls uniformly onto the grid cell.

We denote by A the fraction of the grid cell that is saturated before rainfall begins. The dependence of A on i_0 can be computed from the statistical distribution $f(i)$ via:

$$A(i_0) = \int_0^{i_0} f(i)\, di. \tag{71}$$

Based on these assumptions, for an infinitesimal rain input dP, the state variable i_0 increases by exactly the amount dP, unless $i_0 + dP > i_m$, in which case i_0 increases to its maximum i_m. The increase in total soil water content after the infinitesimal rainfall is

$$dW = [1 - A(i_0)]dP, \tag{72}$$

because only the unsaturated fraction of the grid cell stores additional water. The saturated fraction A will create surface runoff of the amount $dP \times A$. Presuming that this runoff is completely absorbed by the unsaturated fraction of the same grid cell, increases A by the amount

$$dA = \frac{dA}{di_0} dP = f(i_0)\, dP. \tag{73}$$

Integration of Equ. (72) yields an expression of the more commonly used state variable total soil water content, W_0, which can be used to substitute i_0:

$$W_0(i_0) = i_0 - \int_0^{i_0} A(i)\, di. \tag{74}$$

In this integration, the soil is filled from fully dry by a series of infinitesimal amounts di until the amount stored locally in the soil reaches either i_0 or its local saturation level. The soil is filled up in the same way as when adding rain, so that dP in Equ. (73) can be substituted by di , and the modified equation be integrated from 0 to i_0. Equ. (74) is valid for $i_0 < i_m$, and i_0 the total amount of water added. The integral over $A(i)$ on the r.h.s. of Equ. (74) is the amount of water lossed when local parts of the soil become saturated.

Similar to the use of $W_0(i_0)$ instead of i_0, i_m does not have to be defined explicitly as a model parameter, but can be derived using the definition $W_c = W_0(i_m)$, with W_c, the moisture storage capacity of the soil at the grid-cell scale, used as the primary model parameter.

Using Equ. (74), we derive direct runoff Q_d for a finite amount of rainfall, P_s, as long as the sum of i_0 and this value is not more than i_m, considering that i_0 increases to $i_0 + P_s$:

$$Q_d = P_s - W_0(i_0 + P_s) + W_0(i_0) = \int_{i_0}^{i_0+P_s} A(i)\, di. \tag{75}$$

Otherwise, the maximum infiltration of the grid cell determines direct runoff:

$$Q_d = P_s - W_0(i_m) + W_0(i_0) = P_s - W_c + W_0. \tag{76}$$

VIC-1L uses the following functional form of the cumulative sub-gridscale distribution of infiltration capacity:

$$A(i) = 1 - (1 - i/i_m)^B \tag{77}$$

With this, we obtain

$$Q_d = P_s - W_c + W_0 + W_c \max\left\{1 - \frac{i_0 + P_s}{i_m}; 0\right\}^{1+B} \tag{78}$$

with

$$i_m = (1+B)W_c \tag{79}$$

and

$$i_0 = i_m \left[1 - \left(1 - \frac{W_0}{W_c}\right)^{\frac{1}{1+B}}\right]. \tag{80}$$

This yields the following expression for infiltration ($I = P_s - Q_d$):

$$I = W_c \left(1 - \max\left\{1 - \frac{i_0 + P_s}{i_m}; 0\right\}^{1+B}\right) - W_0. \tag{81}$$

The VIC-1L model is applied to W_r, i.e. the entirety of the plant-available soil moisture, with the following exceptions:

- Soil evaporation is computed similar to VIC-3L (Liang et al., 1996), where the saturated fraction of the grid cell, $A(i_0)$, evaporates at the potential rate, and the remaining fraction as a function of the surface layer soil moisture. Different to VIC, the surface layer soil moisture of the unsaturated fraction is represented by its average volumetric soil moisture.
- Base flow is computed such that the soil can only drain to W_f instead of 0.
- There is a further thin surface layer containing W_s of water, and with a maximum water storage capacity of $W_{s,c}$.

The base flow equation used by D&B can therefore be written as

$$Q_b = k_b \max\{W_r - W_{r,f}; 0\}, \tag{82}$$

where W_r is the root-zone soil moisture, and $W_{r,f}$ its value at field capacity. $W_{s,c}$ is computed based on the depth of the surface soil layer, d_s, and volumetric soil moisture at saturation (Table 4) via $W_{s,c} = d_s\theta_s$. d_s is set to 4 cm, but limited (in rare cases) to the depth of the soil to bedrock.

It is further assumed that the infiltration capacity of the surface layer varies spatially following Equ. (77), but with B replaced by B_s, i.e. has a different statistical distribution from the root-zone. However, an important, simplifying assumption is that this variation is statistically independent of the spatial variation of infiltration capacity of the root-zone layer. It is thus assumed that if $A(i_0)$ is fractional grid cell area where the soil is saturated, the same fraction $A(i_0)$ of the surface layer is also saturated, but the remaining fraction always has the same statistical distribution, and its average saturated per-area water content is always $W_{s,c}$, independent of $A(i_0)$.

Soil evaporation, E_s, is computed such the actual rate is equal to the potential rate times the ratio between actual and saturated surface-layer soil moisture. Different to VIC-3L, this ratio is based not on the point-wise soil water content, but on the average per-area soil water content of the unsaturated grid cell fraction, i.e. $W_{s,u} = \frac{W_s - A(i_0)W_{s,c}}{1-A(i_0)}$. This assumption leads to the following simple expression:

$$E_s/E_p = A(i_0) + [1 - A(i_0)]\frac{W_{s,u}}{W_{s,c}} = \frac{W_s}{W_{s,c}}. \tag{83}$$

where the potential evaporation rate is assumed as $E_p = E_{eq}$ with the equilibrium evapotranspiration, E_{eq}, according to Jarvis and McNaughton (1986):

$$\lambda E_{eq} = \frac{s(R_n - G)}{s + \gamma} \tag{84}$$

with s from Equ. 144 with $s(T) = \partial e_s/\partial T$ and γ from Equ. 59.

Infiltration, I, is first computed for the root-zone layer, which overlaps with the surface layer and is therefore the infiltration for the entire simulated soil water pool. The same concept of variable infiltration capacity is used to determine how much of I remains in the surface layer, building on the equivalent expression for the root-zone layer (Equ. (81)), but where P_s is replaced by I, B by the specific parameter for the surface layer, B_s, and the resultant values yields the part of infiltration that remains in the surface layer.

Surface soil moisture is updated to the next time steps following the same procedure as for the root-zone layer, which is executed first to compute infiltration. After that, W_s is updated to an intermediate value W_s^+ by subtracting soil evaporation (Equ. (83)) and a term for drainage to below the surface layer, formulated in a similar way to the base flow:

$$W_s^+ = W_s - E_s - Q_s \tag{85}$$

with

$$Q_s = k_s \max\{W_s^+ - W_{s,f}; 0\}. \tag{86}$$

After that, infiltration into the surface layer is calculated based on W_s^+, which is then added to W_s^+ to obtain surface soil moisture at the beginning of the following time step:

$$W_s(t+\Delta t) = W_s^+ + I_s = W_{s,c}\left(1 - \max\left\{1 - \frac{i_{s,0}^+ + I}{(1+B_s)W_{s,c}}; 0\right\}^{1+B_s}\right), \tag{87}$$

with

$$i_{s,0}^+ = (1+B_s)W_{s,c}[1-(1-W_s^+/W_{s,c})^{1/(1+B_s)}]. \tag{88}$$

All fluxes, i.e P_s, Q_d, Q_b, Q_s, are fluxes integrated over the time step of 1 day.

This hydrology scheme has two state variables – surface soil moisture, W_s, and total or root-zone soil moisture, W_r, where W_s is part of W_r – and the following parameters: volumetric soil moisture at saturation, Θ_s and field capacity Θ_f differentiated by soil texture class (Table 4, the same texture class is assumed for both layers), the base flow parameter k_b, the surface drainage parameter k_s, and the shape parameters for the root-zone, B, and for the surface layer, B_s.

Using the depth of the corresponding layer, d_i (d_s for surface, d_r for root-zone layer), $W_{c,i}$ and $W_{f,i}$ of layer i is determined from:

$$W_{c,i} = \Theta_s d_i, \tag{89}$$

for the moisture storage capacity, and

$$W_{f,i} = \Theta_f d_i. \tag{90}$$

for the field capacity.

k_s is simulated from spatially constant base flow drainage rates for 150 mm and 320 mm of $kb_{150} = 0.095$/day and $kb_{320} = 0.032$/day taken from Wood et al. (1992):

$$k_s = (kb_{150} - (150. - W_{c,s}) * (kb_{320} - kb_{150})/(320. - 150.)) * 2.1 \tag{91}$$

We used $k_b = 0.2$/day, and $B_s = 10$, while a spatially-varying B is provided by Gao et al. (2009).

A time step for the entire scheme is executed following the procedure described in Wood et al. (1992), first for the root-zone, then for the surface layer:

1. Base flow from the entire soil moisture store is computed according to Equ. (82).
2. Soil evaporation, E_s, is computed from Equ. (83), based on W_s of the previous time step.
3. From W_r, base flow, soil evaporation and transpiration are subtracted.

Table 4: Assumed volumetric soil moisture at saturation (Θ_s), field capacity (Θ_f) and wilting point (Θ_w) differentiated by texture class.

	Coarse	Medium/Coarse	Medium	Fine/Medium	Fine	Organic
Θ_s	0.410000	0.435000	0.451000	0.420000	0.476000	0.451000
Θ_f	0.193706	0.245704	0.298119	0.303402	0.377204	0.298119
Θ_w	0.071982	0.110032	0.149533	0.170485	0.244554	0.149533

4. Direct runoff, Q_d, is computed from Equ. (78) using the intermediate value of W_r from the previous sub-step replacing W_0. The value of P_{tot} (Equ. 51) is computed as the sum of non-intercepted precipitation, throughfall from the canopy water pool, and snow melt.

5. The value of W_r from the intermediate step is updated by adding P_s and subtracting Q_d to obtain the value of the surface soil moisture at the end of the time step.

6. The value of W_s from the previous step is updated to an the intermediate value W_s^+ (Equ. (85)) by subtracting soil evaporation, E_s, and drainage from the surface layer (Q_s, Equ. (86)).

7. The part of infiltration remaining in the surface layer is is added to W_s^+ to obtain the surface soil moisture at the next time step (Equ. (87)).

The information used by the model's photosynthesis module is the ratio between the total plant-available soil moisture and its value at field capacity, $W_{r,f}$, where plant-available soil moisture equals actual root-zone soil moisture, W_r minus root-zone soil moisture at wilting point, $W_{r,w}$. This value is cut off at both 0 and 1 according to:

$$f_{soil} = \begin{cases} 0 & \text{if} \quad W_r \leq W_{r,w} \\ \frac{W_r - W_{r,w}}{W_{r,f} - W_{r,w}} & \text{if} \quad W_{r,w} < W_r < W_{r,f} \\ 1 & \text{if} \quad W_r \geq W_{r,f} \end{cases} \tag{92}$$

The wilting point soil moisture content is computed using Θ_w from Table 4:

$$W_{w,r} = \Theta_w d_r. \tag{93}$$

In order to simulate the effect of irrigation on cropland soil water balance, we applied a lower threshold for W_r according to of 0.3 to

$$W_r \geq 0.3(W_{r,f} - W_{r,w}) + W_{r,w}. \tag{94}$$

Similarly, for surface layer soil moisture, W_s we applied a threshold of 30% of the field capacity:

$$W_s \geq 0.3 W_{s,f}. \tag{95}$$

1.2.6 Energy balance

Through the energy balance (Equ. 96 and 97), surface temperature and thereby evaporation and transpiration rates are highly dependent upon net radiation, R_n. Consequently, it is in the interest of the plant to absorb sunlight as effectively as possible, while at the same time keeping the absorbed radiative energy, R_n, as small as possible. In fact, plants absorb photosynthetically active light to almost 90% while they reflect or scatter around 90% of the light in the near infrared, which is of no value for photosynthesis. Besides this, through "clumping" and keeping leaves in an erect position, vegetation can reduce light absorption during midday, while increasing it in the morning and the evening when atmospheric demand for transpiration is lowest. To simulate such effects, net radiation and with it the

entire energy balance is split into a vegetation, $R_{n,v}$, and a soil part, $R_{n,s}$. The energy balance for both parts can be written as:

$$R_{n,v} = H_v + \lambda(E_t + E_i) \tag{96}$$

and

$$R_{n,s} - G = H_s + \lambda(E_s + E_{sn}) \tag{97}$$

where H is the sensible heat flux and λ the latent heat of evaporation (see Equ. 64). There are two evaporation fluxes controlled by $R_{n,v}$ (transpiration and skin reservoir evaporation) and two controlled by $R_{n,s}$ (soil and snow evaporation), while both subsystems are linked by a common reservoir, W_s, for the two dominant fluxes, E_t and E_s.

1.2.7 Snow module

The effect of snowfall on the energy and water balance is twofold: On the one hand, snow increases the maximum amount of water that can be stored at the land surfaces; on the other hand, snow, and fresh snow in particular, has a very low albedo, decreasing net radiation at the surface (Equ. 125) and thereby evaporation (Equ. 103). Since snow height enters the calculation of the snow albedo, a simple formulation is included for this variable.

The snow balance is described by the following equation:

$$W_{sn}(t) - W_{sn}(t - \Delta t) = (P_{sn}(t) - S_m(t) - E_{sn}(t))\Delta t \tag{98}$$

The snowfall rate, P_{sn}, depends on the daily average temperature, $\bar{T}$, and the precipitation rate, P_{tot} (Wigmosta et al., 1994):

$$P_{sn} = \begin{cases} P_{tot} & \text{for} \quad \bar{T} \leq -1.1^o\text{C} \\ \frac{3.3-\bar{T}}{4.4} P_{tot} & \text{for} \quad -1.1^o\text{C} < \bar{T} < 3.3^o\text{C} \\ 0 & \text{for} \quad 3.3^o\text{C} \leq \bar{T} \end{cases} \tag{99}$$

For snow melt, a simple function of temperature is chosen (in kg m^{-2}day^{-1} Hagemann and Dümenil, 1996):

$$S_m = 3.22 \max\{\bar{T}; 0\} \text{ kg m}^{-2}\text{day}^{-1} \tag{100}$$

with $\bar{T}$ in ^{o}C. Since $W_{sn}(t)$ in Equ. 98 is not allowed to assume negative values, the maximum for S_m is given by

$$S_m(t)\Delta t \leq W_{sn}(t - \Delta t) + (P_{sn}(t) - E_{sn}(t))\Delta t \tag{101}$$

Equilibrium evaporation (cf. Equ. 84) is taken for the potential snow evaporation rate, $E_{sn,max}$, derived from the energy input to the ground, $R_{n,s} - G$ (Equs. 127 and 128, cf. Equ. 97), with the latent heat of sublimation (λ, Equ. 64) and the slope of the vapour pressure curve above ice (s, see Equ. 144, for γ see Equ. 59):

$$\lambda E_{sn,max} = \frac{s(R_{n,s} - G)}{s + \gamma} \tag{102}$$

$E_{sn,max}$ is thus determined primarily by net radiation, $R_{n,s}$, and depends to a large extent on snow albedo. The daily snow evaporation cannot exceed the amount of snow on the ground plus the snowfall:

$$E_{sn}(t)\Delta t = \min\{E_{sn,max}(t)\Delta t; \quad W_{sn}(t - \Delta t) + P_{sn}(t)\Delta t\} \tag{103}$$

with a time step Δt of one day. We assume snow sublimation at the equilibrium rate, which results from the Penman-Monteith equation (Equ. 58) in the limit $G_a \to 0$.

When calculating the snow balance, the snowfall rate is first determined (P_{sn}, Equ. 99), then the evaporation rate E_{sn} from Equ. 103. Once these two variables are known, the limitation of the rate of snow melt, S_m (Equ. 100), can be determined from the relationship 101. Finally, the updated value for the snow pool size, W_{sn}, is calculated from Equ. 98.

Snow height, h_{sn}, is calculated from old-snow, ξ_{sn}, and fresh-snow density, ξ^n_{sn}:

$$h_{sn} = \frac{max\{W_{sn} - P_{sn} + E_{sn}, 0\}}{\xi_{sn}} + \frac{max\{P_{sn} - E_{sn}, 0\}}{\xi^n_{sn}} \tag{104}$$

with ξ^n_{sn} in kg m^{-3} (Loth and Graf, 1996):

$$\xi^n_{sn} = \begin{cases} 30 & \text{for} \quad \bar{T} \leq -22.5^o\text{C} \\ 10 + \frac{8}{3}(\bar{T} + 30) & \text{for} \quad -22.5^o\text{C} < \bar{T} \leq -15^o\text{C} \\ 50 + 1.7(\bar{T} + 15)^{1.5} & \text{for} \quad \bar{T} > -15^o\text{C} \end{cases} \tag{105}$$

and daily average temperature, $\bar{T}$, in ^{o}C.

Assuming vertically uniform density, i.e.

$$\xi_{sn}(t - \Delta t) = \frac{W_{sn}(t - \Delta t)}{h_{sn}(t - \Delta t)} \tag{106}$$

density of old snow is computed with a compaction rate by Anderson (1976) as follows:

$$\xi_{sn}(t) = \xi_{sn}(t - \Delta t) \left(1 + \frac{g}{\eta^0_c} \exp\left[-a_c \xi_{sn}(t - \Delta t) + b_c T\right] \frac{W_{sn}(t - \Delta t)\Delta t}{2}\right) \tag{107}$$

The constants are set according to the recommendations of Anderson (1976): $\eta^0_c = 3.7{\times}10^7$ kg m^{-1} s^{-1}, $a_c = 2.1{\times}10^{-2}$m ^{3} kg^{-1} and $b_c = 8{\times}10^{-2}$ K^{-1}. In Equ. 104 a floor value of 10^{-9} kg m^{-3} is used for the densities of old and new snow.

1.2.8 Radiation balance

The radiative balance at the surface is computed in five steps:

1. Actual shortwave (solar) incoming radiation, R_{sw} is used as input.
2. Solar elevation, earth-sun distance, solar flux and height above sea level are computed from geographical position, Julian day and hour (UTC) and taken as input to the computation of potential solar incoming radiation in both the photosynthetically active (PAR) and near-infrared (NIR) domains.
3. Potential NIR (R^{pot}_{NIR}) and photosynthetically active incoming radiation (R^{pot}_{PAR}) in combination with actual solar incoming radiation are used to calculate actual incoming PAR, R_{PAR}.
4. The ratio r_{sw} of potential to actual incoming solar radiation is used to calculate the direct fraction of incoming PAR, as opposed to diffuse incoming PAR clouds and atmospheric scattering.
5. The radiative balance at both vegetated and bare-soil surfaces are calculated using incoming shortwave radiation (R_{sw}), LAI (Λ), fractional cover (f_c) and air temperature (T).

The second step begins with the computation of the inverse squared earth-sun distance in astronomical units, $r^{-2}_{\odot}$ (ie. in units of the average distance) according to Paltridge and Platt (1976):

$$\begin{aligned} r^{-2}_{\odot} \quad = \quad & 1.00011 + 0.034221\cos(\alpha_0) + \ldots \\ & 0.0128\sin(\alpha_0) 0.000719\cos(2\alpha_0) + \ldots \\ & 0.000077\sin(2\alpha_0) \end{aligned} \tag{108}$$

with $\alpha_0 = 2\pi(d-1)/365$ and the Julian day d (1: January 1st; 365: December 31st). Solar elevation, μ, defined as the cosine of the angle between zenith and the position of the sun (i.e. $\mu = 1$ if the sun stands at zenith and $\mu = 0$ if the sun is at the horizon), is computed in the following way:

$$\mu = \sin(\phi)\sin(\delta) - \cos(\phi)\cos(\delta)\cos(t\pi/12) \tag{109}$$

ϕ is the latitude, $\delta = -23.4(\pi/180)\cos(2\pi(d+10)/365)$ is the position of the sun within the ecliptic, and t local solar time in hours. The solar flux above the atmosphere through a plane parallel to the earth's surface, R_{OA}, is given by

$$R_{OA} = S_0 r_\odot^{-2} \mu \tag{110}$$

with the solar constant $S_0 = 1360$ Wm^2. If $\mu < 10^{-3}$, incoming radiation is neglected and treated as zero.

In the second step, PAR at the surface, R_{PAR}, is first calculated following Weiss and Norman (1985):

$$R_{PAR} = R_{sw} \frac{R_{PAR}^{pot}}{R_{PAR}^{pot} + R_{NIR}^{pot}} \tag{111}$$

with R_{sw} incoming shortwave radiation (a driving variable). Potential PAR is computed as

$$R_{PAR}^{pot} = t_{PAR} S_{0,PAR} r_\odot^{-2} \mu \tag{112}$$

with the total PAR transmittance

$$t_{PAR} = 0.4 + (1 - 0.4\mu) t_{PAR,D} \tag{113}$$

and the PAR transmittance for direct radiation under clear skies

$$t_{PAR,D} = \exp\left(\frac{0.185}{\mu}\frac{p}{p_0}\right). \tag{114}$$

The transmittance for diffuse incoming PAR is

$$t_{PAR,d} = t_{PAR} - t_{PAR,D} = 0.4 - 0.4\mu t_{PAR,D}. \tag{115}$$

Potential near infrared radiation (NIR) is computed as

$$R_{NIR}^{pot} = t_{NIR} S_{0,NIR} r_\odot^{-2} \mu \tag{116}$$

with the total NIR transmittance

$$t_{NIR} = t_{NIR,D} + 0.6\left(1 - t_{NIR,D}\mu - \frac{w_{NIR}}{S_{0,NIR}}\right), \tag{117}$$

and the direction NIR transmittance

$$t_{NIR,D} = \exp\left(-\frac{0.06}{\mu}\frac{p}{p_0}\right) - \frac{w_{NIR}}{S_{0,NIR}} \tag{118}$$

Diffuse NIR transmittance is again defined as the remainder:

$$t_{NIR,d} = t_{NIR} - t_{NIR,D}, \tag{119}$$

and w_{NIR} is the water absorption in the NIR for 10 mm of precipitable water:

$$w_{NIR} = S_0 \times 10^{-1.1950 + 0.4459\log_{10}(1/\mu) - 0.0345[\log_{10}(1/\mu)]^2}, \tag{120}$$

where $S_0 = S_{0,PAR} + S_{0,NIR}$. w_{NIR} is further limited by

$$w_{NIR} \leq S_{0,NIR} \exp\left(-\frac{0.06}{\mu}\frac{p}{p_0}\right). \tag{121}$$

The fraction of direct radiation in PAR, d_{PAR}, is also calculated according to Weiss and Norman (1985):

$$d_{PAR} = \left\{ \begin{array}{ll} 0 & \text{for} \quad r_{sw} < 0.2 \\ \left(1 - \left(\frac{0.9 - r_{sw}}{0.7}\right)^{2/3}\right) \frac{t_{PAR,D}}{t_{PAR}} & \text{for} \quad 0.2 < r_{sw} < 0.9 \\ 1 & \text{for} \quad r_{sw} > 0.9 \end{array} \right\}, \tag{122}$$

where

$$r_{sw} = \frac{R_{sw}}{R^{pot}_{PAR} + R^{pot}_{NIR}} \tag{123}$$

is the ratio of actual to potential incoming shortwave radiation.

Further, we have p, the surface air pressure and $p_0 = 1.01325 \times 10^5$ Pa, the reference surface air pressure. p is computed from elevation, h, in m and daily mean temperature, $\bar{T}$, in K with the lapse rate of the standard atmosphere, $\mathcal{L}$ (6×10^{-3} K/m, Houghton, 1986):

$$p = p_0 \left(\frac{1}{1 + h\mathcal{L}/\bar{T}}\right)^{gM_a/(R\mathcal{L})} \tag{124}$$

with the standard surface gravity, g (9.81 m s^{-1}), and M_a, the molar mass of dry air (28.964×10^{-3} kg/mol).

The final step consists of calculating the radiative balance at the surface:

$$R_n = R_{L\downarrow} - R_{L\uparrow} + (1 - \rho_S) R_{sw} \tag{125}$$

where ρ_S stands for surface albedo, $R_{L\downarrow}$ for longwave thermal radiation from the atmosphere to the surface and $R_{L\uparrow}$ for long wave radiation back from the surface. As explained above, net radiation is divided into a vegetation and a soil part ($R_n = R_{n,v} + R_{n,s}$):

$$R_{n,v} = (1 - t_{l,v})(R_{L\downarrow} - R_{L\uparrow} - G) + a_v R_{sw} \tag{126}$$

and

$$R_{n,s} = t_{l,v}(R_{L\downarrow} - R_{L\uparrow}) + (1 - t_{l,v})G + a_s R_{sw} \tag{127}$$

$t_{l,v}$ is the longwave (thermal) transmissivity of vegetation, a_v and a_s the shortwave (solar) effective absorptivity of vegetation and soil, respectively (see Equ. 137), and G the soil heat flux. G must be subtracted from $R_{n,s}$ to obtain the total available energy for evapotranspiration and latent heat loss from the soil (see Equ. 97). According to Verma et al. (1986), G is assumed to be a constant fraction of net radiation (cf. also Rosenberg, 1974, p. 179ff):

$$G = 0.036 R_n \tag{128}$$

It is assumed that the fraction $(1 - t_{l,v})$ of the soil heat flux is equal to the thermal radiation from the vegetation to the soil, so that this amount enters the radiative balances of both vegetation and soil.

Thermal upward radiation from the surface, $R_{L\uparrow}$, is computed from air temperature with a single value for surface emissivity, ε_O, of 0.97 (average for land surfaces, Brutsaert, 1982, p. 137):

$$R_{L\uparrow} = \varepsilon_O \sigma T_K^4 \tag{129}$$

with the Stefan-Boltzmann constant σ (5.6703$\times 10^{-8}$ Wm^{-2}K^{-4}) an the air temperature in Kelvin ($T_K = T + 273.16$), where T is air temperature in degrees Celsius.

Downward thermal radiation, $R_{L\downarrow}$, is computed with a temperature and humidity dependent emissivity of the cloudless atmosphere, ε_A, and a correction term depending on cloudiness, $r_{\varepsilon A}$:

$$R_{L\downarrow} = \varepsilon_A r_{\varepsilon A} \sigma T_K^4 \tag{130}$$

with

$$\varepsilon_A = \varepsilon_{A0} \left(\frac{e_a}{T_K} \right)^{\frac{1}{7}} \tag{131}$$

according to Brutsaert (1982, p. 139), where e_a is given in Pa and T_K in K, with a standard value for ε_{A0} of 0.64, and an average correction from Bolz (1949),

$$r_{\varepsilon A} = 1 + 0.22 n_c^2 \tag{132}$$

Here, cloud fraction, n_c, is estimated from r_{sw} (Equ. 123) following

$$n_c = \begin{cases} 1 & \text{for} \quad r_{sw} < 0.5 \\ (0.9 - r_{sw})/0.4 & \text{for} \quad 0.5 < r_{sw} < 0.9 \\ 0 & \text{for} \quad r_{sw} > 0.9 \end{cases} \tag{133}$$

According to Brutsaert, the standard value for ε_{A0} is 0.64. Since r_{sw} is unknown during nighttime, we use the average of the ratio of actual to potential incoming solar radiation during the preceding day. In this particular case, we define daytime as those hours, where the sun zenith angle is less than 85 degrees. This substitution is applied for all times steps where the sun zenith angle is greater than 85 degrees.

Since thermal radiation is computed from air temperature, T, the effect of warming or cooling of both vegetation and soil surfaces is neglected. This effect can be accounted for by the concept of isothermal conductivity, which is discussed below (Section 1.2.4).

Transmission of radiation through the vegetation canopy is computed from the two-flux equation with zero single-scattering albedo ($\omega = 0$, cf. Section 1.1.3), which is equivalent to Beer's Law of radiation absorption:

$$t_{l,v} = f_c \exp(-\bar{\mu}\Lambda / f_c) + (1 - f_c) \tag{134}$$

with $\bar{\mu} = 1$ and f_c the fractional vegetation cover. In order to insure radiative balance between vegetation and soil, it is further assumed that the fraction $(1 - t_{l,v})$ of the soil heat flux comes from the net radiation of the vegetation canopy (see above).

Absorptivity of vegetation and soil, a_v and a_s, depends in a complex fashion on structure and distribution of the leaves, and on the optical properties of leaves and the soil. Here, both values are estimated on the basis of f_{PAR}, the fraction of absorbed PAR computed in the photosynthesis part of the model (see Equ. 47):

$$a_s = (1 - \rho_s) - (1 - \rho_s - a_{s,0}) f_{PAR} \tag{135}$$

where $a_{s,0} = 0.05$ is the fraction absorbed by the soil under a closed canopy, and

$$a_v = (1 - \rho_v - a_{s,0}) f_{PAR} \tag{136}$$

ρ_v is the albedo of dense vegetation (standard value: 0.15, Brutsaert 1982, p. 136). With these two equations, surface albedo, ρ_S, can be expressed as

$$\rho_S = 1 - a_v - a_s = \rho_s + (\rho_v b - \rho_s) f_{PAR} \tag{137}$$

The given value for $a_{s,0}$ has been found with the two-flux equations for PAR and NIR at medium soil brightness (0.15 and 0.25) and a LAI of 3 (cf. Section 1.1.3). Since the required accuracy for net radiation is lower than for

Table 5: Values for the soil albedo of three different brightness classes according to Wilson and Henderson-Sellers (1985), for both wet ($\rho_{s,w}$) and dry ($\rho_{s,d}$) soils.

brightness class	$\rho_{s,w}$	$\rho_{s,d}$
light	0.18	0.35
medium	0.10	0.20
dark	0.07	0.15

absorption of PAR for photosynthesis calculations, this mode of estimate should be sufficient for the complete range of f_{PAR}. The necessity to solve the two-flux equations for both PAR and NIR is thus avoided.

The value for the soil albedo, ρ_s, depends either on soil water content of the surface layer, W_s, and the brightness class of the soil, or, in the presence of snow (h_{sn}>0, Equ. 104), on snow albedo, ρ_{sn}. In the absence of snow, we have

$$\rho_s = x_w \rho_{s,w} + (1 - x_w)\rho_{s,d} \tag{138}$$

where x_w reflects the wetting status of the surface soil layer. If surface-layer water content is at field capacity or above (i.e. $W_s \geq W_{s,f}$), the wet-soil value is assumed ($x_w = 1$). If the surface soil has dried out completely, the value for dry soils is taken ($x_w = 0$), while for intermediate values of the soil water content, the albedo is linearly interpolated between the two values, with weight

$$x_w = \min\{W_s/W_{s,f}, 1\}. \tag{139}$$

The albedo for wet and dry soils, $\rho_{s,w}$ and $\rho_{s,d}$, listed in Table 5, is determined by the brightness classification by Wilson and Henderson-Sellers (1985), which is part of the input data (see Section 1.4.

If snow is present ($h_{sn} > 0$), ρ_s follows the snow albedo, ρ_{sn}, calculated as in the snow model by Loth and Graf (1996). In this case, the equation is modified according to:

$$\rho_s = (1 - f_{sn})\left(x_w \rho_{s,w} + (1 - x_w)\rho_{s,d}\right) + f_{sn} * \rho_{sn} \tag{140}$$

with $f_{sn} = \min(h_{sn}/0.1, 1)$, the snow albedo ρ_{sn}, and snow height h_{sn}.

ρ_{sn} is a state variable set to the value of wet soil, $\rho_{s,w}$, at the start of a model run. Each time there is snowfall (see Section 1.2.7), ρ_{sn} is increased by $P_{sn}/\xi^n_{sn} \times 10$ m^{-1} after a time step of one day, where P_{sn} is daily snowfall in kg m^{-2} and ξ^n_{sn} the density of fresh snow from Equ. 105. ρ_{sn} is allowed to reach a maximum of 0.8, the albedo of fresh snow. In order to simulate the decrease in snow albedo during aging, its value is decreased after each one-day time step, at a rate depending on daily average temperature, $\bar{T}$. If $\bar{T} < 0$, a constant rate of 0.006 per day is assumed, while for temperatures above freezing the decrease in albedo is also affected by melting and thus depends on snow height, h_{sn}. If h_{sn} lies above a critical value of 25 cm, daily decrease is $0.107 - 0.214\rho_{sn}$, while below that value the daily decrease is 0.071. In addition, it is assured that ρ_{sn} does not fall below the value of the snow-free soil.

1.2.9 Atmospheric humidity

Since no reliable data of near-surface air humidity exist for purposes of global modelling, this quantity has to be estimated. In such cases (e.g. Running et al., 1987) it is often assumed that the daily mean of the vapour pressure is equal to the saturation vapour pressure at the daily minimum temperature. Friend (1998) has investigated this assumption with climate data by Müller (1982) and has found a good agreement for Europe and North America. For weather stations in arid regions, however, agreement is much less satisfactory, resulting in an overall correlation coefficient of $r^2 = 0.87$ for 805 stations. An overestimate of the vapour pressure occurs, when the air is not saturated

at the minimum temperature, T_{min}, as under severe drought (Running et al., 1987), and an underestimate, when the vapour pressure rises during the day because of evapotranspiration (Rosenberg, 1974, p. 132ff).

In order to account for such findings, the daily course of the vapour pressure, $e_a(t)$, is calculated from instantaneous saturation vapour pressure, $e_s(T)$, saturation vapour pressure at sunrise, $e_s(T_{min})$, and the ratio f_e of daily mean evapotranspiration and daily mean evaporative demand. Variation of the dependence is achieved through the parameters h_0 (relative humidity at sunrise, when $T = T_{min}$, and total drought, i.e. $f_e = 0$) and $\hat{h}$ (daily amplitude of the vapour pressure under moist conditions, i.e. $f_e = 1$, as a fraction of the amplitude at constant saturation):

$$e_a = e_{a0} + f_e \hat{h} \left(e_s(T) - e_{a0} \right) \tag{141}$$

where

$$e_{a0} = \left(h_0 + (1 - h_0) f_e \right) e_s(T_{min}) \tag{142}$$

and

$$f_e(t) = \frac{E_{tot}(t - \Delta t)}{E_{t,max}(t - \Delta t) + E_{s,max}(t - \Delta t)} \tag{143}$$

f_e is defined as the ratio of actual evapotranspiration (Equ. 50) to potential evapotranspiration from vegetation (Equ. 65) and soil (Equ. 102). For the computation of e_a, the value of the preceding time step Δt of one day is taken. The saturation vapour pressure over water or ice, $e_s(T)$, is calculated from Murray (1967):

$$e_s(T) = \begin{cases} 610.78 \exp\left(17.269T/(237.3 + T)\right) & \text{for} \quad T > 0 \\ 610.78 \exp\left(22.33T/(271.15 + T)\right) & \text{for} \quad T < 0 \end{cases} \tag{144}$$

e_s is given in units of Pa and T in ^{o}C.

Instead of a dependence on actual evapotranspiration, Friend (1998) has chosen a formulation for the daily mean vapour pressure depending on precipitation rate and daily minimum temperature. The formulation uses separate regression constants for 704 weather stations. The parameters h_0 and $\hat{h}$ area therefore set such that the results with the parametrisation of this model agree with the formulations found by Friend (1998), i.e. $\overline{e_a} = (a + bP) e_s(T_{min})$.

1.3 Carbon Allocation and Cycling

The overall driver of the carbon cycling module is F^t_{NPP}, the NPP flux into the system at time t, which is partitioned into fraction described by factor f_i, where i is the corresponding pool.

1.3.1 Leaf dynamics and phenology

Leaf dynamics is controlled by the leaf onset function Φ_{onset}, which determines flows from the labile to the leaf carbon pool, according to:

$$C^{t+1}_{lab} = (1 - \Phi_{onset}(t, d_{onset}, c_{ronset}))C^t_{lab} + f_{lab} F^t_{NPP} \tag{145}$$

Changes in the labile pool depend on a fractional input from NPP and losses determined during the period of leaf flushing defined by parameters for the day of leaf onset (d_{onset}) and period of labile release (c_{ronset}).

$$\Phi_{onset}(t, d_{onset}, c_{ronset}) = \frac{\sqrt{2}}{\sqrt{\pi}} \cdot \left(\frac{6.9088}{c_{ronset}} \right) \cdot e^{-(sin(\frac{t - d_{onset} - 0.6425 C_{ronset}}{s}) \cdot \frac{\sqrt{2}s}{c_{ronset}})^2} \tag{146}$$

where $s = 365.25/\pi$. For more details on the phenology equations see Bloom and Williams (2015) Appendix A.

The dynamics of leaf area are determined in D&B from the change in leaf mass (C_{fol}). Leaf mass change is a dynamic outcome of allocation to leaves from the labile C pool, causing bud burst, direct allocation from a fraction of current NPP, and timed losses from leaf senescence using the leaf fall function Φ_{fall}.

$$C^{t+1}_{fol} = (1 - \Phi_{fall}(t, d_{fall}, c_{rfall}, c_{lf}))C^t_{fol} + \Phi_{onset}(t, d_{onset}, c_{ronset}))C^t_{lab} + f_{fol} F^t_{NPP} \tag{147}$$

Losses from the foliar pool are linked to specific periods in the annual cycle through parameters for the day of leaf fall (d_{fall}) and period of labile release (c_{rfall}):

$$\Phi_{fall}(t, d_{fall}, c_{rfall}, c_{lf}) = \frac{\sqrt{2}}{\sqrt{\pi}} \cdot \left(\frac{-log(1 - c_{lf})}{c_{rfall}} \right) \cdot e^{-(sin(\frac{t - c_{rfall} + \psi_f}{s}) \cdot \frac{\sqrt{2}s}{c_{rfall}})^2} \tag{148}$$

c_{lf} is the annual leaf loss fraction, related to leaf life span. ψ_f is a fixed offset term (see Bloom and Williams (2015) Appendix A.).

Leaf area index is determined from foliar C and a parameter for leaf mass per area in C units (c_{LMA}, gCm^{-2} leaf area)

$$LAI^t = C^t_{fol}/c_{LMA} \tag{149}$$

1.3.2 Plant and soil carbon turnover

Dynamics of the fine root (fr) and wood pools (wd) are similarly determined by allocation of NPP and by first order turnover:

$$C^{t+1}_{fr} = (1 - \theta_{fr})C^t_{fr} + f_{fr}F^t_{NPP} \tag{150}$$

$$C^{t+1}_{wd} = (1 - \theta_{wd})C^t_{wd} + f_{wd}F^t_{NPP} \tag{151}$$

Allocation to wood (f_{wd}) is determined by difference once allocation to labile, foliage and fine roots are complete.

Litter turnover is driven by both mineralisation to CO_2 and conversion to SOM by decomposition:

$$C^{t+1}_{lit} = (\Phi_{fall}(t, d_{fall}, c_{rfall}, c_{lf}))C^t_{fol} + \theta_{fr}C^t_{fr} + (1 - (\theta_{lit} + \theta_{decomp})e^{\Theta T^t})C^t_{lit} \tag{152}$$

where T^t is air temperature at time t. Litter fall from the foliar and fine root C pools are input to the litter pool, which has a faster turnover than the SOM pool. The litter pool has strongly periodic inputs linked to leaf senescence plus a continuous input from fine root mortality.

Dynamics of SOM are determined by inputs from turnover of the woody and litter pools, and by mineralisation linked to air temperature:

$$C^{t+1}_{SOM} = (1 - \theta_{SOM}e^{\Theta T^t})C^t_{SOM} + \theta_{wd}C^t_{wd} + \theta_{decomp}e^{\Theta T^t}C^t_{lit} \tag{153}$$

Total ecosystem respiration defined as the sum of autotrophic respiration, R_a, using inputs from Equ. 29, and heterotrophic respiration, R_h, which depends on the rate of mineralisation of dead organic matter, litter and soil organic material:

$$R^t_{reco} = R^t_A + R^t_H \tag{154}$$

with

$$R^t_H = (\theta_{lit}C^t_{lit} + \theta_{SOM}C^t_{SOM})e^{\Theta T^t}. \tag{155}$$

1.3.3 Parameter priors

Prior values for the PFT specific parameters related to carbon allocation and cycling were created using the CARDAMOM model-data fusion system (Bloom et al., 2016) for the Finland (Table 6) and Spain sites (Table 7). CARDAMOM was used to calibrate a previous version of DALEC coupled to a water cycle model (Bloom and Williams, 2015; Smallman and Williams, 2019) at the site scale and across two domains of around 500 by 500 km surrounding those sites, at 0.25×0.25 degrees spatial resolution and with a monthly time step for the years 2001 to 2018, inclusive.

This version of DALEC used the Aggregrated Canopy Model (ACM (Williams et al., 1997)) to provide canopy flux inputs rather than BETHY. The analyses were driven with CRU-JRAv2.1 meteorology (Harris, 2019), MODIS

Table 6: D&B parameters relating to carbon balance and phenology used for Sodankylä site, by plant functional type (PFT; Columns 2, 3). Columns 3-8: same D&B parameters, but applicable for the entire northern Scandinavian study region (18^{o}E - 32^{o}E, 65^{o}N - 69^{o}N).

parameter / PFT (#)	EvCn (5)	EShr (7)	TmSg (4)	EvCn (5)	C3Gr (9)	Tundra (11)	WetV (12)
θ_{decomp}	4.60×10^{-4}	3.30×10^{-4}	5.20×10^{-4}	6.80×10^{-4}	2.65×10^{-4}	2.57×10^{-4}	3.20×10^{-4}
f_{fol}	0.118	0.167	0.184	0.090	0.171	0.181	0.156
f_{fr}	0.277	0.32	0.307	0.276	0.44	0.40	0.34
c_{lf}	1.19	1.52	1.09	1.17	1.21	1.19	1.03
θ_{wd}	1.25×10^{-4}	1.32×10^{-4}	1.81×10^{-4}	9.70×10^{-5}	3.03×10^{-4}	3.40×10^{-4}	1.78×10^{-4}
θ_{fr}	0.0072	0.0043	0.0091	0.0064	0.0067	0.0062	0.0073
θ_{lit}	0.0059	0.00132	0.0039	0.0045	0.00126	0.00123	0.00087
θ_{SOM}	1.57×10^{-5}	3.60×10^{-6}	2.33×10^{-5}	2.08×10^{-5}	7.70×10^{-6}	6.90×10^{-6}	4.00×10^{-6}
Θ	0.048	0.040	0.041	0.042	0.040	0.040	0.039
d_{onset}	156.13	69.18	162.31	136.88	178.69	177.78	149.81
f_{lab}	0.136	0.093	0.129	0.146	0.187	0.151	0.258
c_{ronset}	29.28	33.29	31.04	43.76	20.53	23.00	22.28
d_{fall}	230.32	258.47	239.75	232.19	252.41	253.59	249.68
c_{rfall}	50.86	40.57	48.55	58.18	34.74	34.54	45.88
c_{LMA}	36.11	69.86	45.80	41.99	57.28	50.24	62.69
Initial C_{lab}	30.48	3.75	41.87	37.89	27.32	17.06	22.60
Initial C_{fol}	29.29	16.16	34.72	27.04	27.12	20.66	2.82
Initial C_{fr}	17.86	7.72	29.09	31.40	16.85	14.89	8.09
Initial C_{wd}	3072.24	500.70	3992.10	4689.19	613.07	371.10	743.32
Initial C_{lit}	60.24	41.04	153.42	76.40	158.34	101.35	92.53
Initial C_{SOM}	40910.35	34888.61	37511.67	34302.16	44359.82	35311.00	40989.89

burned area (Giglio et al., 2018) and Global Forest Watch forest cover loss (Hansen et al., 2013). The parameters were retrieved based on calibration against time series of leaf area index (Copernicus Service Information (2020)), woody biomass stock information (Santoro, 2021) and an initial soil C stock (Hengl et al., 2017). Due to the availability of field data for specific PFTs, three site-level analyses were further carried out to provide more constrained diagnostics. These sites included an evergreen coniferous (EvCn) forest using field observations from Hyytiälä, Finland (FLUXNET2015 database (`http://fluxnet.fluxdata.org/`, accessed 01/11/2016); Heiskanen et al., 2012), and both C3 grasslands (C3Gr) and evergreen coniferous forest (EvCn) using observations at Majadas de Tietar. These three analyses took advantage of in-situ estimates of NEE data from eddy covariance and field inventories of LAI and biomass. All other PFT parameter priors were selected based on CARDAMOM grid points which had the largest coverage of each target PFT and realistic parameter retrievals (e.g. evergreen PFTs had leaf life spans, c_{lf}, >1 year).

1.4 Model setup

The model requires the following driving variables at an hourly time step over the integration period:

- 2m air temperature (T)
- soil temperature, used as daily mean ($\bar{T}_{ds}$)
- incoming shortwave (solar) radiation (R_{sw})
- incoming longwave (thermal) radiation ($R_{L\downarrow}$)
- precipitation (P_{tot})

Additional inputs are:

- molar ratio of CO_2 in air (C_a)

Table 7: D&B parameters relating to carbon balance and phenology used for Majadas del Tietar site, by plant functional type (PFT; Columns 2, 3). Columns 4-9: same D&B parameters, but applicable for the entire Iberian study region (8.5^{o}W - 2.5^{o}W, 38.5^{o}N - 43^{o}N).

parameter / PFT (#)	TmEv (3)	C3Gr (9)	TmSg (4)	EvCn (5)	EShr (7)	C3Gr (9)	WetV (12)	ArbC (13)
θ_{decomp}	3.04×10^{-4}	2.58×10^{-3}	5.30×10^{-4}	4.80×10^{-4}	5.90×10^{-4}	9.60×10^{-4}	9.10×10^{-4}	7.40×10^{-4}
f_{fol}	0.050	0.36	0.163	0.139	0.193	0.45	0.163	0.278
f_{fr}	0.36	0.71	0.35	0.51	0.62	0.79	0.53	0.74
c_{lf}	1.10	1.01	1.18	1.79	1.23	1.00	1.17	1.00
θ_{wd}	6.60×10^{-5}	7.30×10^{-4}	1.94×10^{-4}	2.08×10^{-4}	4.90×10^{-4}	9.60×10^{-4}	5.00×10^{-4}	7.80×10^{-4}
θ_{fr}	0.0059	0.0087	0.0076	0.0050	0.0099	0.0126	0.0084	0.0117
θ_{lit}	0.0069	0.00055	0.0043	0.0040	0.0042	0.0058	0.0038	0.0042
θ_{SOM}	2.48×10^{-5}	4.00×10^{-5}	3.04×10^{-5}	2.55×10^{-5}	1.83×10^{-5}	1.04×10^{-5}	2.03×10^{-5}	1.55×10^{-5}
Θ	0.051	0.034	0.043	0.042	0.042	0.060	0.045	0.042
d_{onset}	74.31	77.34	139.84	145.00	82.33	104.50	329.86	106.80
f_{lab}	0.220	0.42	0.148	0.107	0.139	0.0308	0.188	0.215
c_{ronset}	74.18	28.09	20.33	20.64	44.56	26.08	38.56	30.95
d_{fall}	157.38	121.97	260.15	268.05	176.29	129.66	151.99	163.70
c_{rfall}	54.63	65.05	96.93	113.03	67.99	63.26	41.56	71.49
c_{LMA}	67.67	46.94	60.25	104.96	104.66	56.52	107.23	45.11
Initial C_{lab}	34.57	60.99	80.62	30.77	32.41	5.16	5.51	40.37
Initial C_{fol}	36.34	24.84	64.07	139.71	73.05	57.56	128.16	11.35
Initial C_{fr}	34.92	10.64	67.02	97.49	30.30	49.35	29.74	18.86
Initial C_{wd}	6737.40	89.57	5962.44	2227.35	415.67	140.53	874.43	127.46
Initial C_{lit}	12.90	16.35	205.51	146.72	51.40	4.17	21.50	49.60
Initial C_{SOM}	11818.84	15469.69	26847.23	19030.57	13952.27	13573.13	12117.49	12847.95

- soil texture class
- PFT distribution
- fractional vegetation cover (f_c)
- elevation (h, to computer air pressure, Equ. 124).

2 The Layered 2-Stream Model

The layered 2-stream model runs in parallel to the two-flux scheme of the photosynthesis part, but being based on the same equations reproduces identical results. It is part of the observation operator for solar-induced fluorescence (SIF).

To simulate the SIF leaving the top of the canopy, we take the Meador and Weaver (1980) solutions to the radiative transfer problem given for the reflectance ($\mathcal{R}_d$) and transmittance ($\mathcal{T}_d$) of discrete canopy layers given diffuse incident light, which in this case, will be the SIF emission from within the layer, to give:

$$\mathcal{R}_d = \frac{\gamma_2[1 - e^{-2k\tau}]}{\tilde{k} + \gamma_1 + (\tilde{k} - \gamma_1)e^{-2k\tau}} \tag{156}$$

$$\mathcal{T}_d = \frac{2e^{-2k\tau}}{\tilde{k} + \gamma_1 + (\tilde{k} - \gamma_1)e^{-2k\tau}} \tag{157}$$

with:

$$\tau = \frac{LAI}{2} \tag{158}$$

Table 8: Parameter space for FAPAR tests. $U(a-b)$ stands for the uniform distribution with boundaries a and b.

Parameter	Distribution
Λ	$-2\ln(1-U(0-1))$
ω	$U(0-1)$
ρ_s	$U(0-1)$

$$\tilde{k} = \sqrt{\gamma_1^2 - \gamma_2^2} \tag{159}$$

$$\gamma_1 = 2\left(1 - \omega(1-\beta)\right), \tag{160}$$

$$\gamma_2 = 2\omega\beta. \tag{161}$$

where β in D&B is always 0.5 (see Equ. 38). These equations are physically consistent with the canopy radiative transfer elsewhere in D&B, but allow for the inclusion of arbitrary emission sources from within canopy layers.

To test the physical consistency we compare the FAPAR calculated by D&B with the same quantity constructed from the L2SM equations. For the case of a black soil the FAPAR is given, trivially, by:

$$\text{FAPAR}_{bs} = 1 - \mathcal{R}_d - \mathcal{T}_d, \tag{162}$$

and for a soil with reflectance ρ_s:

$$\mathcal{R}_d(\rho_s) = \mathcal{R}_d + \frac{\mathcal{T}_d^2 \rho_s}{1 - \mathcal{R}_d \rho_s}, \tag{163}$$

$$\mathcal{T}_d(\rho_s) = \frac{\mathcal{T}_d}{1 - \mathcal{R}_d \rho_s}, \tag{164}$$

$$\text{FAPAR} = 1 - \mathcal{R}_d(\rho_s) - \mathcal{T}_d(\rho_s)(1-\rho_s), \tag{165}$$

We can then compare the FAPAR predicted by the two-flux scheme of D&B to these equations. While D&B uses a value of 0.12 for ω, we use a random sample of values between zero and one, as shown in Table 8, 100 times for both soil cases, leads to the scatter plot given in Figure 1. The near-perfect straight line relationship between the two models indicates that the physics and assumptions in the two models is, for all purposes, the same. We chose a log transform of the uniform distribution (U) to sample LAI as this produces an approximately linear distribution in the resulting FAPAR.

The SIF emitted from each layer that escapes the top of the canopy can be computed as:

$$\mathcal{E}_n = \frac{S_n \mathcal{T}_{d,n}^{+} \left(1 + \mathcal{R}_{d,n}^{'-}\right)}{1 - \mathcal{R}_{d,n}^{'-} \mathcal{R}_{d,n}^{+}}, \tag{166}$$

where S_n is the SIF emitted from layer n, assuming it occurs at the mid–point of the layer. The superscript $+$ and $-$ are used to refer the optical properties of the canopy level above $(+)$ and below $(-)$ the mid-point of layer n. For example, $\mathcal{T}_{d,n}^{+}$ is the transmittance of the canopy above the middle of layer n, $\mathcal{R}_{d,n}^{-}$ is the reflectance of the canopy below the middle of layer n, and includes the reflectance of the soil. The total canopy leaving SIF is then given by:

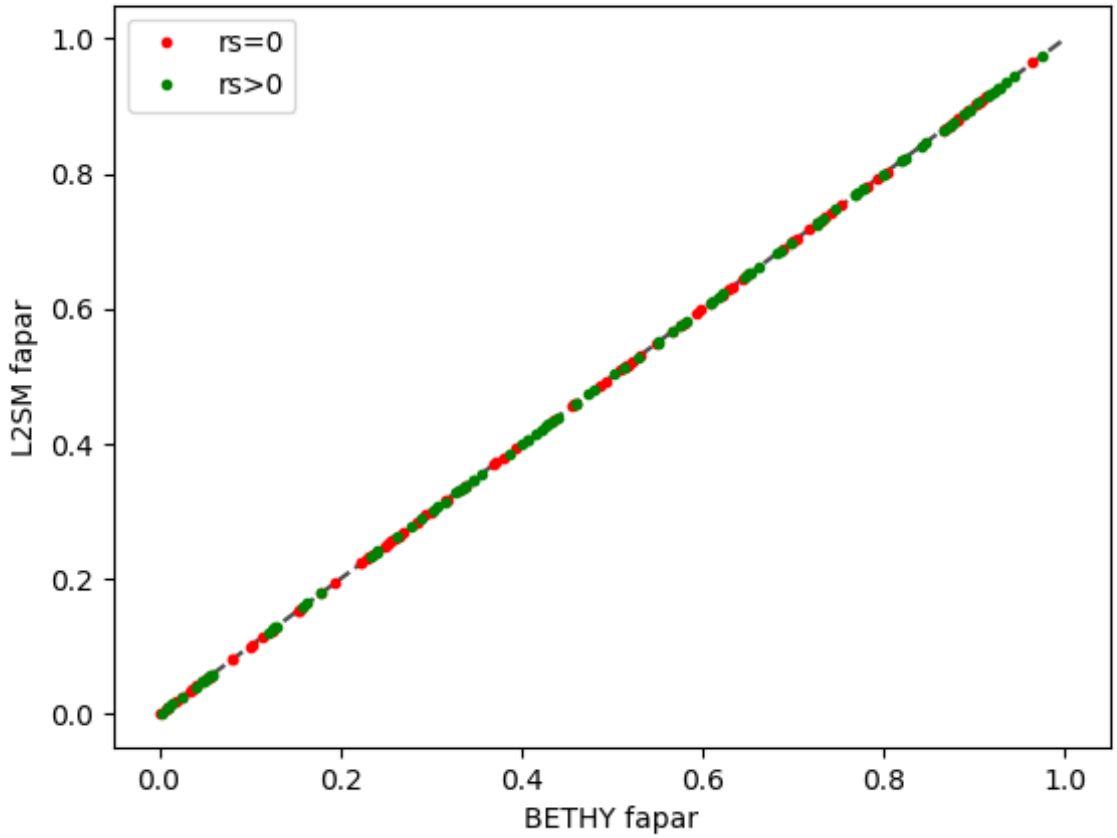

Figure 1: FAPAR predicted by the L2SM and the twoflux scheme of D&B for the case of $\rho_s = 0$ and $\rho_s > 0$. In both cases 100 simulations have been used.

$$\mathcal{E} = \sum_{n=1}^{N} \mathcal{E}_n \tag{167}$$

where N is the number of layers. This formulation explicitly accounts for all levels of SIF photon scattering between the canopy layers and the soil below the canopy, as well as re-absorption within the canopy.

The assumption that the emitted SIF comes from the middle of each layer is valid if the layers are optically thin (i.e. optical properties change proportionally with changes in optical depth) and that SIF is generated uniformly throughout the layer (which is consistent with the photosynthesis routines in D&B, which assume all leaves in a layer are photosynthesising at the same rate). To test the impact of the optically thin assumption we generate 50 different canopies with optical properties sampled according to Table 8 and calculated the total canopy leaving emissions for each canopy dividing it into all possible numbers of layers from 1 to 50. Results are shown in Figure 2 and show the percentage difference from the simulation with 50 layers. Even in the most extreme case, with a single layer, the

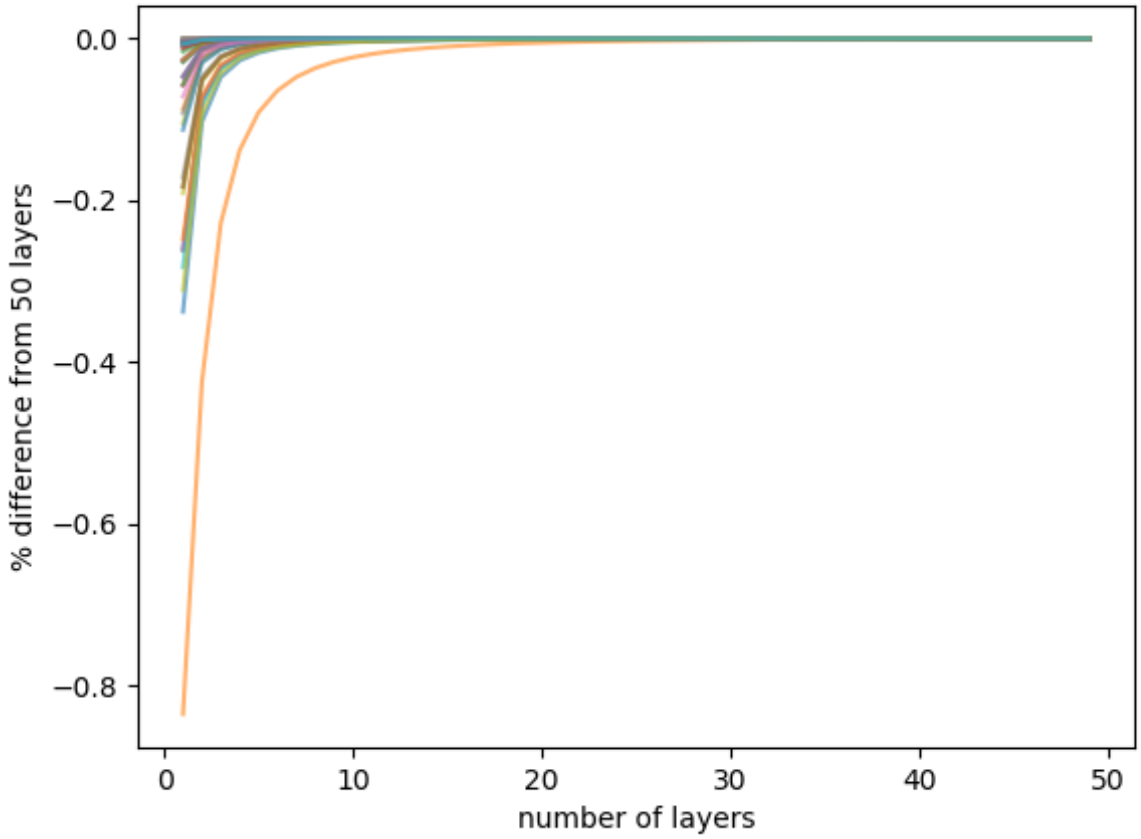

Figure 2: % difference in emissions from 50 random canopies with 1 to 50 layers.

difference is less that 1% from the 50 layer calculation. For three layers (as in D&B) the difference is always less than 0.5% and almost always less the 0.05%. Consequently we can be confident that only very small levels of uncertainty are introduced by this specific assumption.

3 Experimental Methods

3.1 Meteorological variables and radiation

3.1.1 Sodankylä

Air temperature was measured with a Pentronic PT100 thermometer, calibrated every 2-5 years in FMI calibration laboratory, with values averaged to 30 min intervals. Soil temperature was measured at 100 cm depth using a PT100 thermometer and gap filled, and precipitation is measured hourly using Pluvio 2 (OTT HydroMet), as well as daily data from manual rain gauge, calibrated every 2 years.

Short wave incoming and outgoing radiation as well as incoming and outgoing thermal radiation were measured with the NrLite instrument (Kipp & Zonen; Netherlands), with data averaged to 30 minute intervals, using factory calibration.

3.1.2 Majadas del Tietar

Air temperature was measured using the CPK1 5-ME (MELA Sensortechnik; Germany) at m 2 above ground using factory calibration, data averaged for 30 minute intervals, soil temperatures at 80 cm depth below trees or in open grassland using a Th3-s (UMS GmbH, Germany) instrument, and precipitation using tipping bucket 5.4032.45.008 (Thies, Germany), and stored as 60-minute sums. Soil temperature was gap-filled using a random-forest model and used as a model input.

Radiation was measured using ventilated version of CNR4 (Kipp & Zonen; Netherlands) and averaged to 60 minute values. Radiation components, long wave and short wave downwelling and upwelling, were measured for both grass and tree covered areas.

3.2 Eddy covariance observations

3.2.1 Sodankylä

NEE is measured using an eddy covariance system mounted at 22,5 m height, consisting of a sonic anemometer (METEK USA-1 during 2002-2018, and Gill HS-50 during 2018-2021) and a gas analyzers Li-Cor LI-7000 and Li-Cor LI-7200. The sonic anemometers were factory calibrated when purchased. The LI-7000 was calibrated every 2-6 months for zero and span of CO2 and H2O. The LI-7200 was factory-calibrated every 2 years according to the ICOS protocol. SHF was measured using METEK USA-1 (2002-2018) or Gill HS-50 (2018-2021), both using factory calibration.

Standard methods were used for calculating the half-hourly turbulent fluxes (Aubinet et al., 2012). In post-processing, data was screened for low turbulent conditions (u* criterion), non-stationarity (Foken and Wichura, 1996) and instrument failures. The data were then partitioned into GPP and TER and gap-filled by utilizing standard nonlinear regressions for temperature and PAR (Aurela et al., 2015). We therefore need to take into account that the carbon flux measured by the eddy covariance methods is NEE, whereas its decomposition into GPP and TER is derived using a statistical analysis and is therefore dependent on the underlying statistical model.

3.2.2 Majadas del Tietar

NEE was measured using Gill R3-50 ultrasonic-anemometer (Gill; UK) and LI-7200 infrared gas analyser (Licor Bioscience, USA) applying the eddy covariance technique. The Gill R3-50 was factory calibrated in a wind tunnel. The LI7200 was calibrated every half year for zero and span of CO2 and H2O.

Eddy covariance data were collected at 20 Hz with the R3-50 (Gill) and a LI-7200 CO2 and H2O gas analyser (Licor Bioscience) at 15m above ground. Raw data were processed with EddyPro (Fratini and Mauder, 2014) to calculate fluxes of H2O and CO2 at half hourly intervals. Raw data processing steps include de-spiking, planar fit coordinate rotation, lag corrections with default windows and for H2O based on relative humidity classes, high and low frequency corrections were performed. Subsequently, u*-threshold estimation and gap-filling was applied using REddyProc (Wutzler et al., 2018).

The gap-filled timeseries of NEE was partitioned into GPP and Reco by using the night time flux partitioning algorithm of citereichstein2005separation, as implemented in REddyProc. For details of the processing see (El-Madany et al., 2018, 2021).

3.3 Biomass, soil carbon and snow (Sodankylä)

At Sodankylä, 29 soil cores of 50 cm depth were taken in 2011 and analysed every 10 cm for soil organic carbon content. Above-ground biomass was also estimated in 2011 based on a standard forest survey by National Resources Institute of Finland. Diameter at breast height was measured for 700 trees, height for 60 trees, and some trees were cut down. Biomass estimated are therefore based on a combination of allometric equations and direct weighing.

Snow depth was measured regularly at Sodankylä in the forest area around the flux tower using an ultrasonic distance sensor (Campbell Scientific SR50).

3.4 FAPAR and LAI (Sodankylä)

FAPAR was measured at Sodankylä using the PQS1 instrument (Kipp & Zonen; Netherlands) with factory calibration. Four PQS1 sensors were installed in a row below the canopy with a spacing of 5 m. The measurements started on 19 June 2021, as part of the LCC campaign. The below-canopy average (PARb) for these sensors was calculated and compared to the above-canopy PAR measurement (PARa), and FAPAR calculated as (PARa-PARb)/PARa. Results were then calculated as daily averages from daytime data (8:00-14:30 UTC). Simulations correspond to the average of hourly values between 10:00 and 14:00 UTC.

LAI was measured using hemispherical photographs following strict ICOS standards (ICOS, 2021) at four plots at the Sodankylä site on seven dates between 15 June (DOY 166) and 28 September 2022 (DOY 271). For each plot and date, a total of nine photographs were taken. Those photographs were then analyzed with the WinSCANOPY software, employing logarithmic averaging. Another set of LAI measurements were carried out on 28 July 2022 (DOY 209) with the Li-Cor LAI 2200 instrument (LiC-Cor Inc., USA). Light measurements were taken both above and below the canopy. These were used to determine light interception at five different zenith angles. LAI is then computed using a radiative-transfer model provided by Li-Cor. A total of 73 measurements were performed, each consisting of four samples.

3.5 SIF

Measurements at both sites were obtained using a spectrometer, QE, with wavelength ranges 650-800 nm (QE Pro) as part of the Fluorescence Box (JB-Hyperspectral Devices GmbH). The spectrometers has one optical fiber pointing upward and the other pointing downward (tilting angle 5^o from nadir at Sodankylä and 10^o from nadir at Las Majadas), and measure downwelling solar irradiance and reflected radiance from the ground, respectively. The measured reflected radiance also includes the emitted solar-induced fluorescence signal.

Measured raw data were converted into upwelling radiance and downwelling irradiance using spectrometer specific radiometric and spectral calibration coefficients determined in a laboratory calibration. SIF is retrieved from radiance using Frauenhofer line discrimination and spectral fitting methods (Alonso et al., 2008; Cogliati et al., 2015; Cendrero-Mateo et al., 2019) at the O2A (760 nm, far-red) and O2B bands (687 nm, red). The measurements retrieved with solar zenith angle greater 75^o or in unstable illumination conditions were filtered out, and averaged hourly.

3.6 L-VOD (Sodankylä)

Passive L-band VOD was measured at Sodankylä with the Elbara-II instrument (Schwank et al., 2009) at three elevation angles (120^o, 130^o and 140^o). To antennas were employed pointing upwards at the same angle, one placed above the tree canopy on the flux tower, and one below the tree canopy. L-VOD observations were averaged between H and V polarizations.

The measurement geometry of the in-situ L-VOD was changed to increase the biomass in the field of view in two steps, first on 17 September 2021 and then on 14 October 2021, thereby changing the instrument's azimuth angle. The change of estimated biomass density with the field of view of the instrument was substantial for the first change of viewing conditions, increasing from 5 ± 2 kgC/m^3 to 15 ± 5 kgC/m^3. Before the change, the vegetation

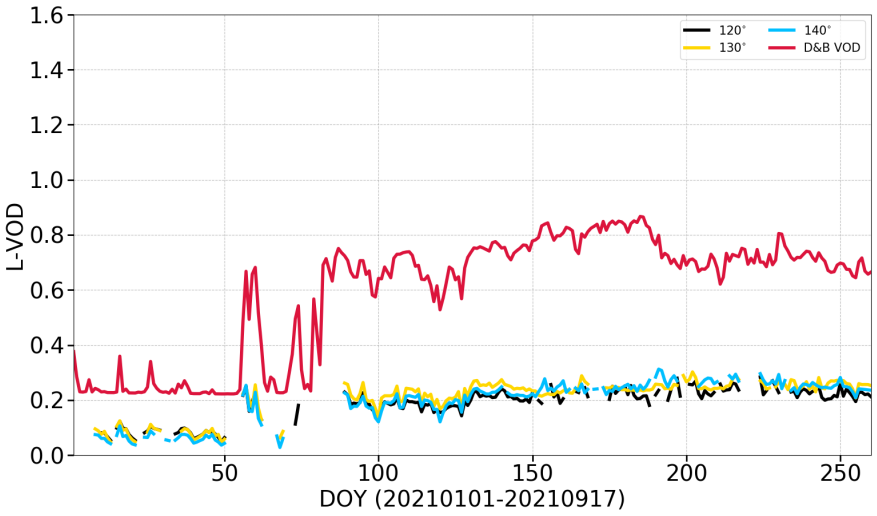

Figure 3: L-band VOD from Elbara II over a pine stand (PFT 5) for different elevation angles compared to D&B simulated L-band VOD, for PFT 5 only, before first change in viewing geometry.

within the field of view was thus estimated to be significantly sparser compared to the wider surroundings, resulting in low measured L-VOD (see Figure 3).

3.7 Soil moisture

At Sodankylä, soil moisture was measured at 5, 10 and 30 cm depth using the ML2-x instrument (Delta-T, UK). At Majadas del Tietar, the ML2-x was used to measure soil moisture ony at 5 cm depth, and measurements at further depths of 10 and 20 cm were measured there using the enviroSCAN SDI12-100 (Sentek Technologies, Australia). The ML-2x sensors use a factory derived cubic function for calculating the soil moisture content. The enviroSCAN instruments have no calibration. Data are saved as 30 minute averages.

At Majadas del Tietar, measurements happened at two positions under tree canopy, and two in open grassland. For Sodankylä the sensor position was the same as that for the soil temperature.

References

Alonso, L., Gomez-Chova, L., Vila-Frances, J., Amoros-Lopez, J., Guanter, L., Calpe, J., and Moreno, J.: Improved Fraunhofer Line Discrimination method for vegetation fluorescence quantification, IEEE Geoscience and Remote Sensing Letters, 5, 620–624, 2008.

Anderson, E. A.: A point energy and mass balance model of a snow cover., NOAA Tec. Rep. NWS 19, US Dept. Commerce, Washington D.C., 150 pp, 1976.

Aubinet, M., Vesala, T., and Papale, D.: Eddy covariance: a practical guide to measurement and data analysis, Springer Science & Business Media, 2012.

Aurela, M., Lohila, A., Tuovinen, J.-P., Hatakka, J., Penttilä, T., and Laurila, T.: Carbon dioxide and energy flux measurements in four northern-boreal ecosystems at Pallas, Boreal Environment Research, 20, 455–473, 2015.

Beerling, D. J. and Quick, W. P.: A new technique for estimating rates of carboxylation and electron transport in leaves of C3 plants for use in dynamic global vegetation models., Global Change Biology, 1, 289–294, 1995.

Bloom, A. A. and Williams, M.: Constraining ecosystem carbon dynamics in a data-limited world: Integrating ecological "common sense" in a model-data fusion framework, Biogeosciences, 12, 1299–1315, https://doi.org/10.5194/bg-12-1299-2015, 2015.

Bloom, A. A., Exbrayat, J. F., Van Der Velde, I. R., Feng, L., and Williams, M.: The decadal state of the terrestrial carbon cycle: Global retrievals of terrestrial carbon allocation, pools, and residence times, Proceedings of the National Academy of Sciences of the United States of America, 113, 1285–1290, https://doi.org/10.1073/pnas.1515160113, 2016.

Bolz, H. M.: Die Abhängigkeit der infraroten Gegenstrahlung von der Bewölkung., Z. Meteorol, 7, 201–203, 1949.

Brutsaert, W.: Evaporation into the atmosphere, Reidel Publishing, Dordrecht, Netherlands, 299 pp, 1982.

Cendrero-Mateo, M. P., Wieneke, S., Damm, A., Alonso, L., Pinto, F., Moreno, J., Guanter, L., Celesti, M., Rossini, M., Sabater, N., et al.: Sun-induced chlorophyll fluorescence III: Benchmarking retrieval methods and sensor characteristics for proximal sensing, Remote sensing, 11, 962, 2019.

Cogliati, S., Verhoef, W., Kraft, S., Sabater, N., Alonso, L., Vicent, J., Moreno, J., Drusch, M., and Colombo, R.: Retrieval of sun-induced fluorescence using advanced spectral fitting methods, Remote Sensing of Environment, 169, 344–357, 2015.

Collatz, G., J.A., B., G.D., F., and J., P.: The relationship between the Rubisco reaction mechanism and models of photosynthesis*, Plant, Cell & Environment, 13, 219–225, https://doi.org/https://doi.org/10.1111/j.1365-3040.1990.tb01306.x, 1990.

Collatz, G., Ball, J., Grivet, C., and Berry, J. A.: Physiological and environmental regulation of stomatal conductance, photosynthesis and transpiration: a model that includes a laminar boundary layer, Agricultural and Forest Meteorology, 54, 107–136, https://doi.org/https://doi.org/10.1016/0168-1923(91)90002-8, 1991.

Collatz, G. J., Ribascarbo, M., and Berry, J. A.: Coupled Photosynthesis-Stomatal Conductance Model For Leaves Of C_4 Plants, Aust. J. Plant Physiol., 19, 519–538, 1992.

Dickinson, R. E., Henderson-Sellers, A., and Kennedy, P. J.: Biosphere-atmosphere transfer scheme (BATS) version 1e as coupled to the NCAR community climate model, NCAR Technical Note NCAR/TN-387+STR., National Center for Atmospheric Research, Boulder, Colorado, 1993.

El-Madany, T. S., Reichstein, M., Perez-Priego, O., Carrara, A., Moreno, G., Martín, M. P., Pacheco-Labrador, J., Wohlfahrt, G., Nieto, H., Weber, U., et al.: Drivers of spatio-temporal variability of carbon dioxide and energy fluxes in a Mediterranean savanna ecosystem, Agricultural and Forest Meteorology, 262, 258–278, 2018.

El-Madany, T. S., Reichstein, M., Carrara, A., Martín, M. P., Moreno, G., Gonzalez-Cascon, R., Peñuelas, J., Ellsworth, D. S., Burchard-Levine, V., Hammer, T. W., et al.: How nitrogen and phosphorus availability change water use efficiency in a Mediterranean savanna ecosystem, Journal of Geophysical Research: Biogeosciences, 126, e2020JG006 005, 2021.

Farquhar, G., von Caemmerer, S. v., and Berry, J.: A biochemical model of photosynthetic CO2 assimilation in leaves of C3 species, Planta, 149, 78–90, 1980.

Farquhar, G. D.: Models relating subcellular effects of temperature to whole plant response, Symposium of the society for Experimental Biology, 42, 395–409, 1988.

Farquhar, G. D. and Sharkey, T. D.: Stomatal conductance and photosynthesis., Ann. Rev. Plant Physiol, 33, 317–345, 1982.

Federer, C.: A soil-plant-atmosphere model for transpiration and availability of soil water, Water Resour. Res., 15, 555–562, 1979.

Federer, C. A.: Transpirational supply and demand: plant, soil, and atmospheric effects evaluated by simulation., Water Resour. Res, 18, 355–362, 1982.

Field, C. and Mooney, H.: The photosynthesis-nitrogen relationship in wild plants, in: On the Economy of Plant form and Function, edited by Givnish, T., pp. 25–55, Cambridge University Press, Cambridge, 1986.

Fischer, R. A. and Turner, N. C.: Plant productivity in the arid and semiarid zones., Ann. Rev. Plant Physiol, 29, 277–317, 1978.

Foken, T. and Wichura, B.: Tools for quality assessment of surface-based flux measurements, Agricultural and forest meteorology, 78, 83–105, 1996.

Fratini, G. and Mauder, M.: Towards a consistent eddy-covariance processing: an intercomparison of EddyPro and TK3, Atmospheric Measurement Techniques, 7, 2273–2281, 2014.

Friend, A. D.: PGEN: an integrated model of leaf photosynthesis, transpiration and conductance., Ecol. Modelling, 77, 233–255, 1995.

Friend, A. D.: Parameterisation of a global daily weather generator for terrestrial ecosystem and biogeochemical modelling., Ecol. Modelling, 109, 121–140, 1998.

Gao, H., Tang, Q., Shi, X., Zhu, C., Bohn, T., Su, F., Sheffield, J., Pan, M., Lettenmaier, D., and Wood, E.: Water budget record from variable infiltration capcity (VIC) model, algorithm theoretical basis document, University of Washington, USA, 2009.

Giglio, L., Boschetti, L., Roy, D. P., Humber, M. L., and Justice, C. O.: The Collection 6 MODIS burned area mapping algorithm and product, Remote Sens. Environ., 217, 72–85, https://doi.org/10.1016/j.rse.2018.08.005, 2018.

Greenland, D. J. and Kowal, J. M.: Nutrient content of the moist tropical forest of Ghana., Plant and Soil, 12, 154–174, 1960.

Hagemann, S. and Dümenil, L.: Development of a parameterization of lateral discharge for the global scale, Technical Report No. 219, Max-Planck-Institut für Meteorologie, Hamburg, 1996.

Hansen, M., Potapov, P., Moore, R., Hancher, M., Turubanova, S., Tyukavina, A., Thau, D., Stehman, S., Goetz, S., Loveland, T., and et al.: High-Resolution Global Maps of 21st-Century Forest Cover Change, Science, 342, 850–853, 2013.

Harris, I.: A forcings dataset of gridded land surface blend of Climatic Research Unit (CRU) and Japanese reanalysis (JRA) data; Jan.1901 - Dec.2017, Dataset, University of East Anglia Climatic Research Unit, "Centre for Environmental Data Analysis",, https://doi.org/10.5285/13f3635174794bb98cf8ac4b0ee8f4ed, 2019.

Heiskanen, J., Rautiainen, M., Stenberg, P., Mõttus, M., Vesanto, V.-H., Korhonen, L., and Majasalmi, T.: Seasonal variation in MODIS LAI for a boreal forest area in Finland, Remote Sensing of Environment, 126, 104–115, https://doi.org/https://doi.org/10.1016/j.rse.2012.08.001, 2012.

Hengl, T., Mendes de Jesus, J., Heuvelink, G., Ruiperez Gonzalez, M., Kilibarda, M., Blagotić, A., Shangguan, W., Wright, M., Geng, X., Bauer-Marschallinger, B., and et al.: SoilGrids250m: Global gridded soil information based on machine learning, PLoS ONE, 12, 2017.

Houghton, J. T.: The Physics of Atmospheres, Cambridge University Press, Cambridge, 271 pp, 2nd edn., 1986.

ICOS: Instructions for Ancillary Vegetation Measurements in Forest: Green Area Index, Aboveground Biomass, Litter Biomass, Tech. rep., 2021.

Jarvis, P. G.: The interpretation of variations in leaf water potential and stomatal conductance found in canopies in the field., Philos. Trans. R. Soc. London, pp. 593–610, 1976.

Jarvis, P. G. and McNaughton, K.: Stomatal control of transpiration: scaling up from leaf to region, Advances in Ecological Research, 15, 1–49, 1986.

Jones, H. G.: Plants and Microclimate, Cambridge University Press, Cambridge, 323 pp, 1983.

Kattge, J. and Knorr, W.: Temperature acclimation in a biochemical model of photosynthesis: a reanalysis of data from 36 species, Plant, Cell & Environment, 30, 1176–1190, https://doi.org/https://doi.org/10.1111/j.1365-3040.2007.01690.x, 2007.

Kelliher, F. M., Leuning, R., and Schulze, E.-D.: Evaporation and canopy characteristics of coniferous forests and grasslands., Oecologia, 95, 152–163, 1993.

Kelliher, F. M., Leuning, R. R., R., M., and E.-D., S.: Maximum conductances for evaporation from global vegetation types., Agric. For. Meteorol, 73, 1–16, 1995.

Knorr, W.: Satellitengestützte Fernerkundung und Modellierung des Globalen CO_2 -Austauschs der Landvegetation: Eine Synthese, Ph.D. thesis, Max-Planck-Institut für Meteorologie, Hamburg, Germany, 1997.

Liang, X., Wood, E., and Lettenmaier, D.: Surface soil moisture parameterization of the VIC-2L model: evaluation and modification, Glob. Planet. Change, 13, 195–206, 1996.

Lindroth, A. and Halldin, S.: Numerical analysis of pine forest evaporation and surface resistance., Agric. For. Meteorol, 38, 59–79, 1986.

Loth, B. and Graf, H.: Modelling the snow cover for climate studies, Tech. Rep. 190, Max-Planck-Institut für Meteorologie, Hamburg, Germany, 1996.

Lugo, A. E. and Murphy, P. G.: Nutrient dynamics of a Puerto Rican subtropical dry forest, Journal of Tropical Ecology, 2, 55–72, 1986.

Meador, W. and Weaver, W.: Two-stream approximations to radiative transfer in planetary atmospheres: A unified description of existing methods and a new improvement, Journal of Atmospheric Sciences, 37, 630–643, 1980.

Monteith, J. L.: Evaporation and environment., Symposium of the Society for Experimental Biology, 19, 205–234, 1965.

Morison, J.: Intercellular CO_2 concentration and stomatal response to CO_2, in: Stomatal Function, edited by Zeiger, E., Farquhar, G. D., and Cowan, I. R., pp. 229–251, Stanford University Press, Stanford, U.S.A, 1987.

Müller, M. J.: Selected climatic data for a global set of standard stations for vegetation science, Junk, Den Haag, Netherlands, 1982.

Murray, F. W.: On the computation of saturation vapour pressure., J. Appl. Meteorol, 6, 203–204, 1967.

Paltridge, G. W. and Platt, C. M.: Radiative Processes in Meteorology and Climatology, Elsevier Publishing, New York, 1976.

Paruelo, J. M. and Lauenroth, W. K.: Relative abundance of plant functional types in grasslands and shrublands of North America., Ecol. Appl, 6, 1212–1224, 1996.

Price, J. C. and Bausch, W. C.: Leaf area index estimation from visible and near-infrared reflectance data., Remote Sens. Environ, 52, 55–63, 1995.

Rosenberg, N. J.: Microclimate: The Biological Environment, Wiley, New York, 315 pp, 1974.

Running, S., Nemani, R., and R., H.: Extrapolation of synoptic meteorological data in mountainous terrain and its use for simulating forest evapotranspiration and photosynthesis., Canadian J. Forestry Res, 17, 472–483, 1987.

Ryan, M. G.: Effects of climate change on plant respiration., Ecol. Appl, 1, 157–167, 1991a.

Ryan, M. G.: A simple method for estimating gross carbon budgets of vegetation in forest ecosystems., Tree Physiol, 9, 255–266, 1991b.

Santoro, M.; Cartus, O.: ESA Biomass Climate Change Initiative (Biomass_cci): Global datasets of forest above-ground biomass for the years 2010, 2017 and 2018, v2., Dataset, University of East Anglia Climatic Research Unit, "Centre for Environmental Data Analysis",, 2021.

Scholze, M., Kaminski, T., Knorr, W., Blessing, S., Vossbeck, M., Grant, J., and Scipal, K.: Simultaneous assimilation of SMOS soil moisture and atmospheric CO_2 in-situ observations to constrain the global terrestrial carbon cycle, Remote Sensing of Environment, 180, 334–345, 2016.

Schulze, E.-D.: Carbon dioxide and water exchange in response to drought in the atmosphere and in the soil., Ann. Rev. Plant Physiol, 13, 127–141, 1986.

Schulze, E.-D., Turner, N. C., Gollan, T., and Shackel, K. A.: Stomatal Response to air humidity and to soil drought, in: Stomatal Function, edited by Zeiger, E., Farquhar, G. D., and Cowan, I. R., pp. 311–321, Stanford University Press, Stanford, U.S.A, 1987.

Schulze, E.-D., Kelliher, F. M., Körner, C., Lloyd, J., and Leuning, R.: Relationships among maximum stomatal conductance, ecosystem surface conductance, carbon assimilation rate, and plant nitrogen nutrition: a global ecology scaling exercise., Ann. Rev. Ecol. Syst, 25, 629–660, 1994.

Schwank, M., Wiesmann, A., Werner, C., Mätzler, C., Weber, D., Murk, A., Völksch, I., and Wegmüller, U.: ELBARA II, an L-band radiometer system for soil moisture research, Sensors, 10, 584–612, 2009.

Sellers, P., Randall, D., Collatz, G., Berry, J., Field, C., Dazlich, D., Zhang, C., Collelo, G., and Bounoua, L.: A Revised Land Surface Parameterization (SiB2) for Atmospheric GCMS. Part I: Model Formulation, Journal of Climate, 9, 676 – 705, https://doi.org/10.1175/1520-0442(1996)009⟨0676:ARLSPF⟩2.0.CO;2, 1996.

Sellers, P. J.: Canopy reflectance, photosynthesis and transpiration, International Journal of Remote Sensing, 6, 1335–1372, https://doi.org/10.1080/01431168508948283, 1985.

Sharkey, D. T. and Ogawa, T.: Stomatal Responses to Light, in: Stomatal Function, edited by Zeiger, E., Farquhar, G. D., and Cowan, I. R., pp. 195–208, Stanford University Press, Stanford, U.S.A, 1987.

Smallman, T. L. and Williams, M.: Description and validation of an intermediate complexity model for ecosystem photosynthesis and evapotranspiration: ACM-GPP-ETv1, Geoscientific Model Development, 12, 2227–2253, https://doi.org/10.5194/gmd-12-2227-2019, 2019.

Turner, N. C.: Adaptation to water deficits: a changing perspective., Aust. J. Plant Physiol, 13, 175–190, 1986.

Turner, N. C., Schulze, E.-D., and Gollan, T.: The responses of stomata to vapour pressure deficits and soil water content, I, pp. 338–342, 1984.

Verma, S. B., Baldocchi, D. D., Anderson, D. E., Matt, D. R., and Clement, R. J.: Eddy fluxes of CO_2, water vapor and sensible heat over a deciduous forest., Boundary Layer Meteorol, 36, 71–91, 1986.

Weiss, A. and Norman, J. A.: Partitioning solar radiation into direct and diffuse, visible and near-infrared components., Agric. For. Meteorol, 34, 205–213, 1985.

Wigmosta, M. S., Vail, L., and Lettenmaier, D. P.: A distributed hydrology-vegetation model for complex terrain., Water Resour. Res, 30, 1665–1679, 1994.

Williams, M., Rastetter, E., Fernandes, D., Goulden, M., Shaver, G., and Johnson, L.: Predicting gross primary productivity in terrestrial ecosystems, Ecological Applications, 7, 882–894, 1997.

Wilson, M. F. and Henderson-Sellers, A.: A Global Archive Of Land Cover And Soils Data For Use In General-Circulation Climate Models, Journal of Climatology, 5, 119–143, 1985.

Wood, E., Lettenmaier, D., and Zartarian, V.: A land-surface hydrology parameterization with subgrid variability for general circulation models, J. Geophys. Res., 97, 2717–2728, 1992.

Woodward, F. I.: Climate and Plant Distribution, Cambridge University Press, Cambridge, 1987.

Wutzler, T., Lucas-Moffat, A., Migliavacca, M., Knauer, J., Sickel, K., Šigut, L., Menzer, O., and Reichstein, M.: Basic and extensible post-processing of eddy covariance flux data with REddyProc, Biogeosciences, 15, 5015–5030, 2018.